

Functional HPV-specific PD-1⁺ stem-like CD8 T cells in head and neck cancer

<https://doi.org/10.1038/s41586-021-03862-z>

Received: 31 August 2020

Accepted: 28 July 2021

Published online: 01 September 2021

 Check for updates

Christiane S. Eberhardt^{1,2,3,4,16}, Haydn T. Kissick^{1,2,5,6,16}, Mihir R. Patel^{5,7}, Maria A. Cardenas⁶, Nataliya Prokhnevskaya⁶, Rebecca C. Obeng^{1,2,8,9}, Tahseen H. Nasti^{1,2}, Christopher C. Griffith^{5,8}, Se Jin Im^{1,2,10}, Xu Wang¹¹, Dong M. Shin^{4,11}, Mary Carrington^{12,13}, Zhuo G. Chen^{5,11}, John Sidney¹⁴, Alessandro Sette^{14,15}, Nabil F. Saba^{5,11}, Andreas Wieland^{1,2,17}✉ & Rafi Ahmed^{1,2,5,17}✉

T cells are important in tumour immunity but a better understanding is needed of the differentiation of antigen-specific T cells in human cancer^{1,2}. Here we studied CD8 T cells in patients with human papillomavirus (HPV)-positive head and neck cancer and identified several epitopes derived from HPV E2, E5 and E6 proteins that allowed us to analyse virus-specific CD8 T cells using major histocompatibility complex (MHC) class I tetramers. HPV-specific CD8 T cells expressed PD-1 and were detectable in the tumour at levels that ranged from 0.1% to 10% of tumour-infiltrating CD8 T lymphocytes (TILs) for a given epitope. Single-cell RNA-sequencing analyses of tetramer-sorted HPV-specific PD-1⁺ CD8 TILs revealed three transcriptionally distinct subsets. One subset expressed *TCF7* and other genes associated with PD-1⁺ stem-like CD8 T cells that are critical for maintaining T cell responses in conditions of antigen persistence. The second subset expressed more effector molecules, representing a transitory cell population, and the third subset was characterized by a terminally differentiated gene signature. T cell receptor clonotypes were shared between the three subsets and pseudotime analysis suggested a hypothetical differentiation trajectory from stem-like to transitory to terminally differentiated cells. More notably, HPV-specific PD-1⁺TCF-1⁺ stem-like TILs proliferated and differentiated into more effector-like cells after in vitro stimulation with the cognate HPV peptide, whereas the more terminally differentiated cells did not proliferate. The presence of functional HPV-specific PD-1⁺TCF-1⁺CD45RO⁺ stem-like CD8 T cells with proliferative capacity shows that the cellular machinery to respond to PD-1 blockade exists in HPV-positive head and neck cancer, supporting the further investigation of PD-1 targeted therapies in this malignancy. Furthermore, HPV therapeutic vaccination efforts have focused on E6 and E7 proteins; our results suggest that E2 and E5 should also be considered for inclusion as vaccine antigens to elicit tumour-reactive CD8 T cell responses of maximal breadth.

Chronic viral infections and cancer result in compromised CD8 T cell function characterized by the expression of several inhibitory receptors including PD-1^{1–5}. Blockade of the PD-1 inhibitory pathway enhances T cell function and is an effective treatment for several cancers^{1,2,5}. Preclinical studies have characterized a unique PD-1⁺TCF-1⁺ stem-like subset of CD8 T cells that maintains the CD8 T cell response during chronic infection and provides the proliferative burst after

PD-1 directed immunotherapy^{6–11}. Similar PD-1⁺TCF-1⁺ CD8 T cells have been found in human tumours^{12–14}. However, a better definition of their antigen specificity and their lineage relationship with other CD8 T cell subsets in the tumour is needed for understanding T cell differentiation pathways in human cancer and to optimize immunotherapeutic approaches. Here we address these questions by analysing HPV-specific CD8 T cells in head and neck squamous cell carcinoma (HNSCC).

¹Emory Vaccine Center, Emory University School of Medicine, Atlanta, GA, USA. ²Department of Microbiology and Immunology, Emory University School of Medicine, Atlanta, GA, USA. ³Centre for Vaccinology, University Hospitals Geneva, Geneva, Switzerland. ⁴Division of General Pediatrics, Department of Pediatrics, Gynecology & Obstetrics, Faculty of Medicine, University of Geneva, Geneva, Switzerland. ⁵Winship Cancer Institute of Emory University, Atlanta, GA, USA. ⁶Department of Urology, Emory University School of Medicine, Atlanta, GA, USA. ⁷Department of Otolaryngology, Emory University School of Medicine, Atlanta, GA, USA. ⁸Department of Pathology, Emory University School of Medicine, Atlanta, GA, USA. ⁹Robert H. Lurie Comprehensive Cancer Center, Northwestern University Feinberg School of Medicine, Chicago, IL, USA. ¹⁰Department of Immunology, Sungkyunkwan University School of Medicine, Suwon, South Korea. ¹¹Department of Hematology and Medical Oncology, Emory University School of Medicine, Atlanta, GA, USA. ¹²Basic Science Program, Frederick National Laboratory for Cancer Research in the Laboratory of Integrative Cancer Immunology, National Cancer Institute, Bethesda, MD, USA. ¹³Ragon Institute of MGH, MIT and Harvard, Boston, MA, USA. ¹⁴Division of Vaccine Discovery, La Jolla Institute for Immunology, La Jolla, CA, USA. ¹⁵Department of Medicine, University of California, San Diego, La Jolla, CA, USA. ¹⁶These authors contributed equally: Christiane S. Eberhardt, Haydn T. Kissick. ¹⁷These authors jointly supervised this work: Andreas Wieland, Rafi Ahmed. ✉e-mail: andreas.wieland@emory.edu; rahmed@emory.edu

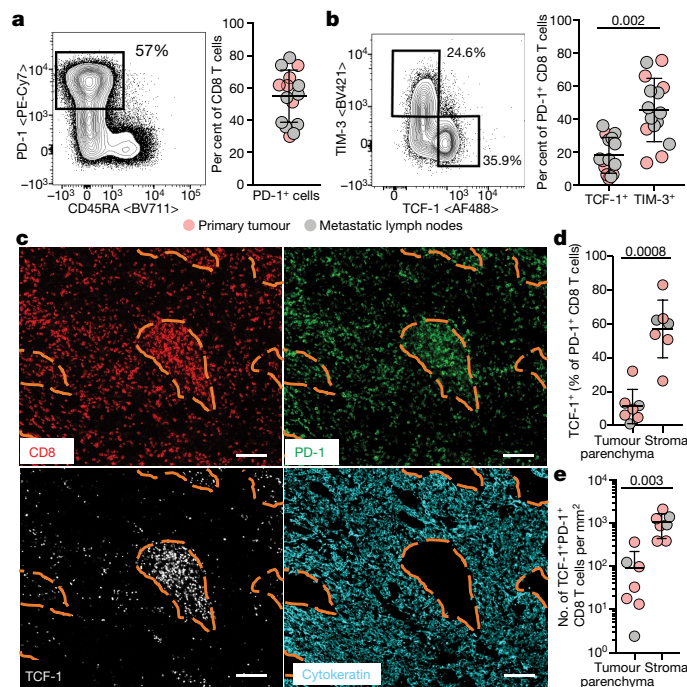


Fig. 1 | Intratumoral PD-1⁺ CD8 T cells are made up of distinct subsets with PD-1⁺TCF-1⁺ stem-like cells residing in lymphoid-like stromal areas.
a, Frequency of PD-1⁺ cells among CD8⁺ TILs. Flow plot is gated on CD8 T cells.
b, Frequency of TCF-1⁺TIM-3⁻ and TIM-3⁺TCF-1⁻ subsets in PD-1⁺ CD8 TILs, with mean and s.d. Two-sided Wilcoxon matched-pairs rank test. Flow plot is gated on PD-1⁺ CD8 T cells. **c**, Representative multiplex immunohistochemistry staining of one of five primary HPV-positive HNSCC tumours with orange dashed lines highlighting parenchyma (cytokeratin⁺) and stromal borders. Scale bars, 100 μm. **d, e**, Frequency (**d**) and density (**e**) of PD-1⁺TCF-1⁺ CD8 TILs in the tumour parenchyma and stroma, with mean and s.d. *n* = 7 (five primary tumours (pink) and two metastatic lymph nodes (grey)). Two-sided paired *t*-tests.

Characterization of CD8 TILs in HNSCC

To investigate the CD8 T cell response to HNSCC, we characterized TILs from six primary tumours and eight metastatic lymph nodes of twelve patients from our treatment-naïve HPV-positive HNSCC cohort. CD8 T cells comprised around 30% of TILs by flow cytometry (Extended Data Fig. 1a). The majority of CD8 TILs expressed high levels of PD-1 and all of the PD-1⁺ cells were CD45RA-negative (Fig. 1a). These PD-1⁺CD45RA⁻ CD8 T cells included distinct populations that expressed either TCF-1 or TIM-3 (Fig. 1b), markers that are commonly used to distinguish stem-like (TCF-1⁺TIM-3⁻) and terminally differentiated (TIM-3⁺TCF-1⁻) PD-1⁺ CD8 T cells^{6–8,14}. Although ranging widely between patients, on average 45% of PD-1⁺ cells exhibited a terminally differentiated phenotype. Stem-like PD-1⁺TCF-1⁺ CD8 T cells were present in all patients and expressed significantly lower levels of granzyme B, Ki-67 and CD39 compared to TIM-3⁺ cells (Fig. 1b, Extended Data Fig. 1b, c). Both subsets expressed TOX (Extended Data Fig. 1d), a key transcription factor for CD8 T cell differentiation during chronic viral infections and cancer¹⁵. We next examined the anatomical location of these PD-1⁺ CD8 T cell subsets in primary tumours and metastatic lymph nodes using multiplex immunohistochemistry. CD8⁺ and PD-1⁺ cells were diffusely present in the cytokeratin-positive tumour parenchyma as well as in the stroma within and around the tumour bed (Fig. 1c, Extended Data Fig. 1e, f). Notably, PD-1⁺TCF-1⁺ cells were predominantly found in the stromal areas and were rarely present in the tumour parenchyma (Fig. 1d, e), whereas the more differentiated cells were diffusely dispersed in the tumour microenvironment (TME) (Extended Data Fig. 1g, h), suggesting that

the stem-like cells reside in distinct niches within the TME and stay away from the tumour itself.

Identification of HPV-specific CD8 TILs

HPV-positive HNSCC offers the opportunity to identify and characterize tumour-reactive CD8 T cells using a defined set of virus-derived tumour-associated antigens. We focused on the known HPV oncogenes E5, E6 and E7, and on E2, which is involved in the episomal maintenance of the HPV genome. To identify HPV-derived CD8 T cell epitopes, we cultured peripheral blood mononuclear cells (PBMCs) from patients with HNSCC with a pool of 251 predicted HPV peptides for 2 weeks and then tested the reactivity of T cells in the expanded PBMCs using interferon-γ (IFNγ) enzyme-linked immunosorbent spot (ELISpot) assays, intracellular cytokine staining (ICCS) and tetramer staining (Fig. 2a, b, Extended Data Fig. 2a–c). Overall, 43 different peptides were identified by ELISpot (22 HPV E2 peptides, 10 HPV E5 peptides, 9 HPV E6 peptides and 2 HPV E7 peptides), with several epitopes being recognized by T cells from multiple patients (Extended Data Fig. 2a). Using patient-specific HLA-typing information, peptide–HLA pairs were predicted in silico and confirmed by in vitro HLA-binding assays, which resulted in the identification of nine CD8 T cell epitopes and the production of seven different MHC class I tetramers, with epitopes derived from HPV E2, E5 and E6 (Extended Data Fig. 2d). Some of the E2, E5 and E6 epitopes that we identified in these patients have also been described in previous studies^{16,17}.

HPV-specific CD8 T cells were readily detectable ex vivo by tetramer staining of TILs isolated from primary tumours and metastatic lymph nodes, and all of these cells expressed high levels of PD-1 (Fig. 2c, Extended Data Fig. 3). The frequency of HPV-specific CD8 T cells varied between patients, ranging from 0.1% to 10% of CD8 TILs, but CD8 T cells to a given epitope were present at similar frequencies in primary tumour and metastatic lymph nodes of the same individual (Fig. 2c, d). In contrast to readily detectable HPV-specific CD8 T cells in the TME, the frequencies of tetramer-positive CD8 T cells in patient-matched peripheral blood were very low (less than 0.02% of CD8 T cells). These results suggest that most HPV-specific CD8 T cells are resident in the TME and do not circulate in the blood, which is consistent with previous reports in various cancers that have shown extremely low frequencies of tumour-specific CD8 T cells in peripheral blood^{16–19}. The uniformly high expression of PD-1 among HPV-specific CD8 TILs suggests that the respective antigens (E2, E5 and E6) are expressed and being presented within the TME. Together, these data show that HPV-specific CD8 T cells can account for a substantial proportion of CD8 TILs in HPV-positive HNSCC, and that although cells of the same antigen specificity can be expanded from PBMCs, their frequency in the blood under steady state conditions is much lower.

Three subsets of HPV-specific CD8 TILs

We sorted HPV tetramer-positive CD8 TILs from seven primary tumours and six metastatic lymph nodes to high purity (Extended Data Fig. 4a, b) and examined their transcriptional signature by single-cell RNA sequencing (scRNA-seq). HPV-specific CD8 TILs comprised three transcriptionally distinct clusters that differed from each other in the expression of several hundred genes (Fig. 3a, Extended Data Fig. 5a–c). All clusters expressed *TOX*—a transcription factor that is critical for establishing an ‘exhausted’ epigenetic state in T cells¹⁵—and the inhibitory molecules *PDCD1*, *CTLA4* and *TIGIT* (Fig. 3b). Cluster 1 cells were characterized by high levels of expression of *TCF7*, a transcription factor essential for the generation of stem-like CD8 T cells during chronic viral infection^{6,7}. Cluster 1 cells also expressed *LEF1*, another transcription factor associated with stem-like T cells; *IL7R*, which is needed for T cell survival; *CCR7*, the primary receptor involved in homing to lymphoid tissue; and *XCL1* and *GPRI83* (EBI2), two molecules involved in migration

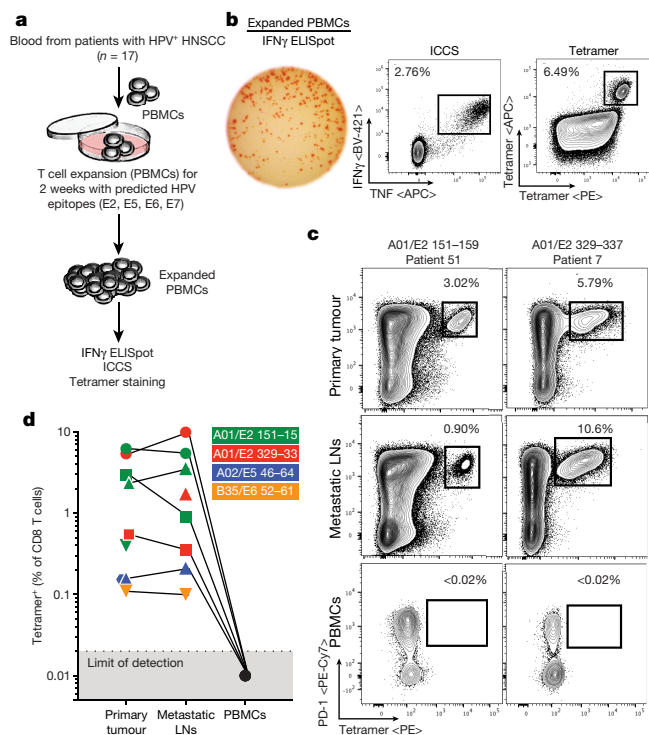


Fig. 2 | Identification of HPV-specific CD8 T cells in PBMCs and tumours of patients with HPV-positive HNSCC. **a**, Schematic of experimental strategy to map HPV-specific CD8 T cell epitopes. **b**, Representative example of expanded PBMCs of an HLA-A*01:01⁺ individual stimulated with HPV E2₃₂₉₋₃₃₇ peptide and analysed by IFN γ ELISpot (left) or ICCS (middle), or stained with the respective tetramer (right). Flow plots are gated on CD8 T cells. **c**, Representative flow plots of ex vivo tetramer-stained CD8 TILs from primary tumour, metastatic lymph nodes (LNs) and PBMCs of two patients. Flow plots are gated on CD8 T cells. **d**, Direct ex vivo frequency of tetramer-positive CD8 T cells in primary tumours, metastatic lymph nodes and PBMCs. Colours indicate different tetramers. Matched samples are connected by lines.

towards and the recruitment of dendritic cells. Of note, effector molecules such as granzymes and perforin were minimally expressed in cluster 1. The HPV-specific CD8 T cells in cluster 2 were characterized by high expression of *PRDM1* and several other transcription factors commonly associated with acute T cell receptor (TCR) engagement such as *NR4A1* (NUR77), *FOS* and *JUN*, and expressed the highest levels

of *IFNG*. Expression of effector molecules such as *GZMA*, *GZMB*, *PRF1* and *GZMY* was found in both clusters 2 and 3, and these clusters also expressed inhibitory receptors such as *HAVCR2* (TIM-3) and *ENTPD1* (CD39). Given the similarity of these HPV-specific CD8 T cell clusters to the stem-like and terminally differentiated CD8 T cells identified in preclinical mouse models, we performed gene set enrichment analyses using gene sets derived from the mouse model of chronic lymphocytic choriomeningitis virus (LCMV) infection⁶. HPV cluster 1 was highly enriched for genes expressed by LCMV-specific PD-1⁺TCF-1⁺ stem-like CD8 T cells (Extended Data Fig. 5e), whereas clusters 2 and 3 exhibited the highest enrichment score for the terminally differentiated gene signature (Extended Data Fig. 5e). Notably, cluster 2 showed high levels of enrichment for both signatures, suggesting that these cells might represent an intermediate population between the stem-like and terminally differentiated states. Thus, we will refer to the three HPV clusters as stem (cluster 1), transitory (cluster 2) and terminally differentiated (cluster 3).

The above analysis included HPV-specific CD8 T cells from different patients, from primary and metastatic sites, as well as different epitope specificities. A separate analysis of HPV-specific CD8 TILs showed a comparable distribution of these cells among the identified clusters independent of sample origin and epitope specificity (Fig. 3c, Extended Data Fig. 4c–e). Furthermore, separate clustering of HPV-specific CD8 TILs from primary tumours and metastatic lymph nodes yielded comparable clusters with minimal differences in gene expression between the corresponding clusters (Extended Data Fig. 5d), suggesting highly similar differentiation states of HPV-specific CD8 TILs in primary and metastatic sites. Flow cytometric analyses of HPV-specific PD-1⁺ CD8 TILs further confirmed the presence of TCF-1⁺ stem-like and more terminally differentiated cells in the TME, with TCF-1⁺ cells expressing high levels of the co-stimulatory molecule CD28 and low levels of granzyme B and TIM-3 (Extended Data Fig. 5f).

It was of interest to determine how total PD-1⁺ CD8 TILs compared to the HPV-specific CD8 T cells. scRNA-seq of total PD-1⁺ CD8 TILs showed that three of the clusters (1–3) were highly similar to the clusters seen in HPV-specific CD8 T cells, but that the total PD-1⁺ CD8 T cells in the tumour had an additional fourth cluster with a distinct transcriptional signature (Extended Data Fig. 6a–e). The origin of these cells is not clear but they could be bystander CD8 T cells that are specific for other viruses^{20,21}.

HPV-specific CD8 T cell subsets share TCRs

The TCR repertoire of HPV-specific CD8 TILs showed dominance of TCR clonotypes for each tetramer (Extended Data Fig. 7b, c). Paired scRNA-seq data from the primary and metastatic site for individual

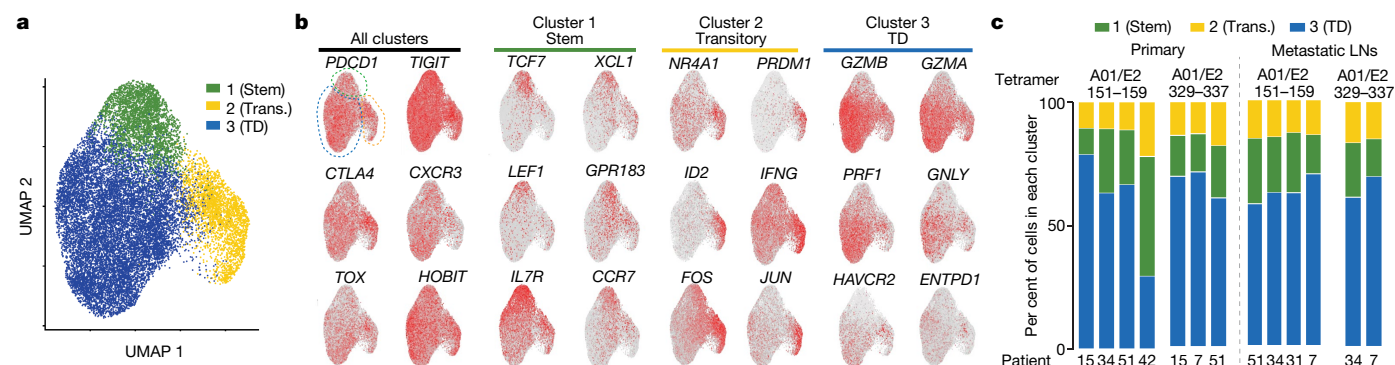


Fig. 3 | HPV-specific CD8 TILs are made up of three transcriptionally distinct clusters. **a**, UMAP analyses of HPV tetramer-specific CD8 T cells (around 20,000 cells) from 13 samples were combined and 3 distinct clusters were identified: cluster 1 (stem-like), cluster 2 (transitory; trans.) and cluster 3

(terminally differentiated or exhausted; TD). **b**, UMAP plots showing the expression of selected genes. **c**, Relative distribution of clusters for each patient and tetramer.

patients showed a correlation between the frequency of a given clonotype in the two sites (Extended Data Fig. 7c, d). Most importantly, HPV-specific CD8 T cells showed a notable degree of TCR clonal overlap between the three clusters (Fig. 4, Extended Data Fig. 7e, f). In fact, the most dominant as well as less dominant clonotypes were similarly distributed among the stem-like, transitory and terminally differentiated HPV-specific CD8 T cells (Extended Data Fig. 7g). This was seen for all of the HPV-specific tetramer-sorted CD8 T cells that we analysed.

Lineage relationship of HPV-specific CD8 TIL subsets

Give the observed TCR overlap between the different clusters, we investigated a potential lineage relationship between the distinct HPV-specific CD8 T cell states present in the tumour using pseudotime analyses. These analyses showed that CD8 T cells that start from a stem-like state (cluster 1) would transition through cluster 2 with a more effector-like signature before reaching a terminally differentiated state (cluster 3), while progressively losing the stem-like signature (Extended Data Fig. 8a–c). This analysis also showed that the relative proportion of a given TCR clonotype was evenly distributed across the stem-like, transitory and terminally differentiated states of the pseudotime progression, suggesting that there is no preference for cells to remain in certain transcriptional states based on their TCR clonotype (Extended Data Fig. 8d).

To provide direct experimental evidence of the proposed lineage relationship model, we examined the potential of HPV-specific PD-1⁺ stem-like and the more terminally differentiated CD8 T cells to proliferate and differentiate after stimulation with the cognate HPV peptide *in vitro*. We took TILs directly from the tumour, labelled them with CellTrace Violet (CTV) and then sorted CTV-labelled CD8 TILs by flow cytometry, on the basis of the expression of the surface markers PD-1, TIM-3 and CD39, into stem-like (PD-1⁺TIM-3⁺CD39⁻) and terminally differentiated (PD-1⁺TIM-3⁺CD39⁺) CD8 T cells (Fig. 5a, Extended Data Fig. 9a). Of note, stem-like cells obtained through this gating strategy expressed high levels of TCF-1 (Extended Data Fig. 9a). The two sorted PD-1⁺ subsets were then cultured for five days in the presence of patient-matched autologous PBMCs pulsed with the tetramer-specific HPV-derived peptide. In the absence of the HPV peptide, there was minimal to no proliferation of either the stem-like or the terminally differentiated CD8 T cells isolated from the tumour (Fig. 5b). However, stimulation of the stem-like cells with HPV peptide resulted in extensive proliferation of the HPV-specific tetramer-positive CD8 T cells, with these cells undergoing up to seven divisions. In contrast, only minimal to no proliferation was observed when the terminally differentiated HPV-specific CD8 T cells were stimulated with the same peptide-pulsed PBMCs (Fig. 5b). The superior proliferative capacity of HPV-specific stem-like CD8 T cells was observed for all seven samples as measured by the replicative index—a measure of the number of divisions the cell undergoes after antigen stimulation (Fig. 5c). These results clearly show that the HPV-specific PD-1⁺ stem-like CD8 T cells present in the tumour have proliferative potential, whereas the more differentiated HPV-specific CD8 T cells have lost the ability to divide after antigen stimulation.

We next investigated whether the antigen-induced proliferation of HPV-specific stem-like CD8 T cells was associated with differentiation into more effector-like and terminally differentiated cells. Stem-like CD8 T cells cultured in the absence of antigenic stimulation expressed low levels of TIM-3, granzyme B, and CD39, thus maintaining their *in vivo* phenotype (Fig. 5d). However, stimulation of these HPV-specific stem-like CD8 T cells with the cognate HPV peptide resulted in marked upregulation of TIM-3, granzyme B and CD39 by the tetramer-positive proliferating CD8 T cells (Fig. 5d). CD25 expression also increased on these dividing HPV-specific CD8 T cells (Extended Data Fig. 9b). In marked contrast, the terminally differentiated HPV-specific CD8 T cells did not proliferate after antigen stimulation, retained high levels of

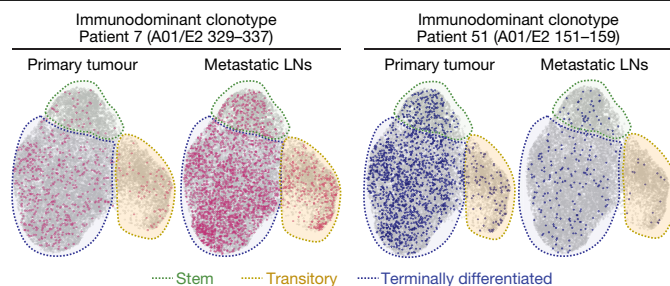


Fig. 4 | The three HPV-specific transcriptionally distinct clusters share TCR clonotypes. Dominant TCR clonotypes specific for a given tetramer are present in all three HPV-specific CD8 T cell subsets (stem-like, transitory and terminally differentiated).

TIM-3, granzyme B and CD39 (Fig. 5d) and only showed minimal upregulation of CD25 (Extended Data Fig. 9b). Both the stem-like and the terminally differentiated HPV-specific CD8 T cells expressed CD45RO, and expression of this molecule did not change after peptide stimulation (Extended Data Fig. 9b). It is worth noting that the HPV-specific PD-1⁺ stem-like CD8 T cells expressed the CD45RO isoform and are distinct from the human stem-cell-like memory CD8 T (T_{SCM}) cells that were defined on the basis of CD45RA expression²².

In addition to the acquisition of markers associated with a more differentiated state, the HPV-specific stem-like cells also decreased the expression of surface markers that are associated with the stem-like state. HPV-specific PD-1⁺ stem-like CD8 T cells that were cultured without antigenic stimulation expressed IL-7R, a cytokine receptor providing critical signals for cell survival, but downregulated their expression of IL-7R after antigen-induced proliferation (Fig. 5d). Stem-like CD8 T cells cultured in the absence of antigenic stimulation maintained expression of CD28—an important co-stimulatory molecule required for the proliferative burst upon PD-1 blockade²³—whereas terminally differentiated cells did not express significant levels of CD28 (Extended Data Fig. 9b). Notably, antigen stimulation of stem-like CD8 T cells resulted in the retention of CD28 expression by many of the dividing cells (Extended Data Fig. 9b).

Together, these studies clearly demonstrate that HPV-specific PD-1⁺TCF-1⁺ stem-like CD8 TILs—in contrast to more differentiated cells—have the ability to proliferate and differentiate into more effector-like CD8 T cells after antigenic stimulation, and could act as resource cells to maintain HPV-specific CD8 T cell responses in patients with HNSCC.

Implications

Our findings have implications in three main areas: first, for PD-1-based therapy of patients with HPV-positive HNSCC; second, for HPV therapeutic vaccination strategies; and third, for viral-mediated cancers in general.

First, we show that the cellular machinery for responding to PD-1 directed immunotherapy is present in patients with HPV-positive HNSCC. Functional HPV-specific PD-1⁺TCF-1⁺ CD8 T cells that can proliferate and differentiate into effector-like cells after antigen stimulation were readily detectable in the tumours of these patients. Definitive studies in preclinical mouse models have shown that this subset of CD8 T cells provides the proliferative burst of effector-like T cells after PD-1 blockade and there is also evidence suggesting that the presence of these PD-1⁺TCF-1⁺ CD8 T cells in human tumours correlates with responsiveness to PD-1 therapy^{6–8,12}. Patients with HPV-positive HNSCC who had undergone conventional treatments and then relapsed have shown low response rates to PD-1 therapy²⁴. Our results now provide a strong rationale for further investigation of PD-1 targeted neoadjuvant and adjuvant therapies in HPV-positive head and neck cancer. Of

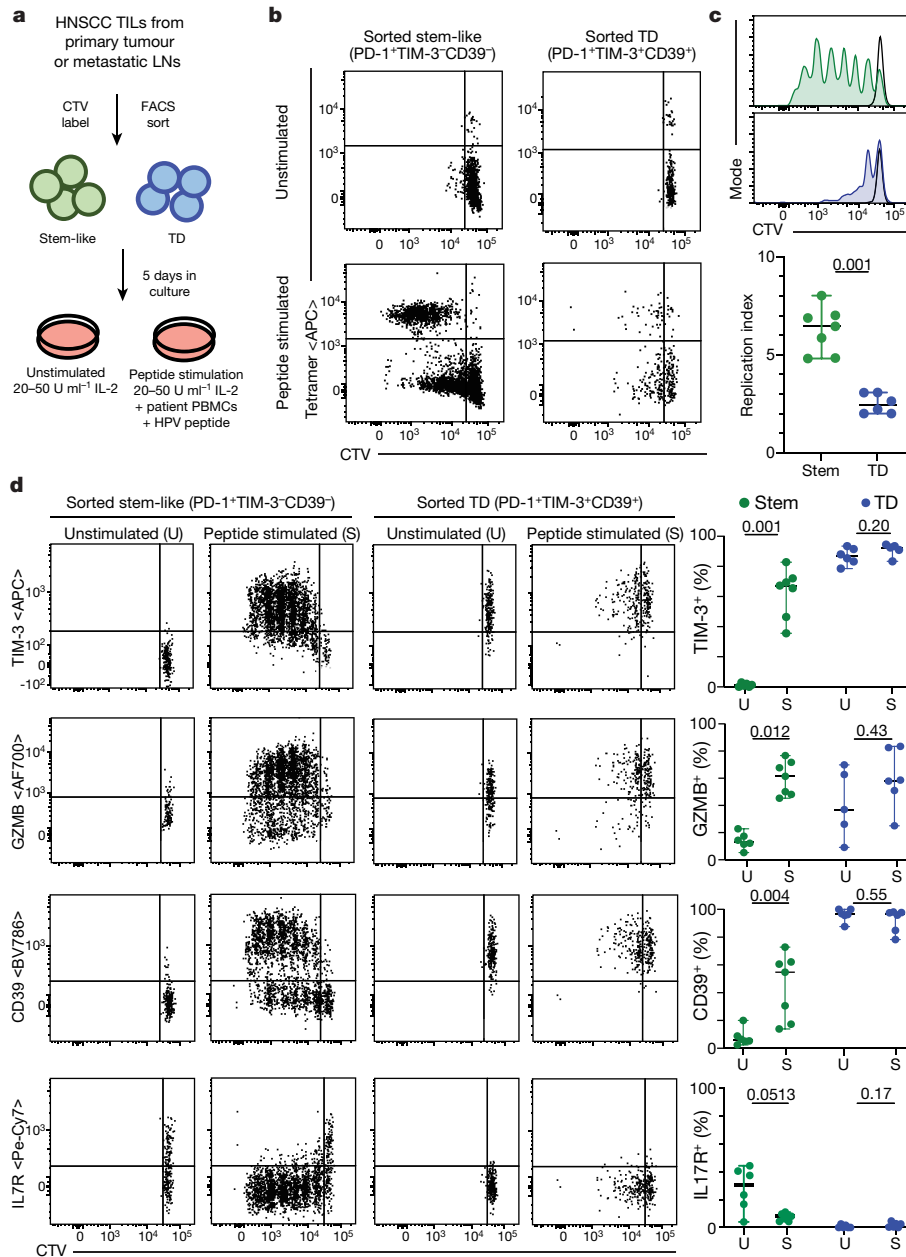


Fig. 5 | HPV-specific PD-1⁺TCF-1⁺ stem-like CD8 T cells in the tumour have proliferative capacity and can differentiate into effector-like cells.

a, Experimental design to isolate stem-like and terminally differentiated subsets from the tumour and test the proliferative and differentiation capacity of HPV-specific CD8 T cells. **b**, Representative plots show HPV-tetramer staining and CTV dilution of stem-like and terminally differentiated cells after five days of culture with autologous PBMCs in the presence or absence of

HPV-specific peptide. **c**, Replication index of stem-like ($n = 7$) and terminally differentiated ($n = 6$) cells. Histograms show representative CTV dilution of tetramer-specific CD8 T cells. **d**, Representative plots showing CTV dilution and expression of selected markers after five days of stimulation with HPV-specific peptide (S) or unstimulated with no peptide (U). Summary plots show the percentage of cells expressing the indicated markers. Mean and s.d.; two-sided unpaired Mann-Whitney U test.

note, our studies were done in treatment-naive patients, whereas the PD-1 clinical trials that showed low responsiveness were done in patients with HNSCC who had received extensive previous treatments (radiation, chemotherapy and surgery) that may have reduced the number of HPV-specific T cells. Future PD-1 therapy trials should take this into consideration.

Second, there have been considerable efforts in developing therapeutic HPV vaccines for patients with cancer but most of these studies have focused on HPV E6 and E7 as the target antigens for the vaccine²⁵. Our studies now show that E2 and E5 are major targets of the intratumoral CD8 T cell response in patients with HPV-positive HNSCC. Thus, therapeutic vaccination strategies for patients with HPV-positive

HNSCC should, in addition to E6 and E7, also consider including E2 and E5 as vaccine antigens to elicit tumour-reactive CD8 T cell responses of maximal breadth. This vaccine-induced response could be further enhanced by concurrent PD-1 blockade, which has previously been shown to synergize with therapeutic vaccination in a preclinical chronic infection model²⁶.

Finally, it is important to emphasize that viral-mediated cancers are a major public health problem worldwide²⁷. Our study characterizing the CD8 T cell response in patients with HPV-positive HNSCC, along with another study that examined HPV-specific B cell responses in the same patients²⁸, can serve as benchmarks for the analysis of immune responses in other viral-mediated cancers.

Online content

Any methods, additional references, Nature Research reporting summaries, source data, extended data, supplementary information, acknowledgements, peer review information; details of author contributions and competing interests; and statements of data and code availability are available at <https://doi.org/10.1038/s41586-021-03862-z>.

1. Hashimoto, M. et al. CD8 T cell exhaustion in chronic infection and cancer: opportunities for interventions. *Annu. Rev. Med.* **69**, 301–318 (2018).
2. McLane, L. M., Abdel-Hakeem, M. S. & Wherry, E. J. CD8 T cell exhaustion during chronic viral infection and cancer. *Annu. Rev. Immunol.* **37**, 457–495 (2019).
3. Gallimore, A. et al. Induction and exhaustion of lymphocytic choriomeningitis virus-specific cytotoxic T lymphocytes visualized using soluble tetrameric major histocompatibility complex class I-peptide complexes. *J. Exp. Med.* **187**, 1383–1393 (1998).
4. Zajac, A. J. et al. Viral immune evasion due to persistence of activated T cells without effector function. *J. Exp. Med.* **188**, 2205–2213 (1998).
5. Barber, D. L. et al. Restoring function in exhausted CD8 T cells during chronic viral infection. *Nature* **439**, 682–687 (2006).
6. Im, S. J. et al. Defining CD8⁺ T cells that provide the proliferative burst after PD-1 therapy. *Nature* **537**, 417–421 (2016).
7. Utzschneider, D. T. et al. T cell factor 1-expressing memory-like CD8⁺ T cells sustain the immune response to chronic viral infections. *Immunity* **45**, 415–427 (2016).
8. He, R. et al. Follicular CXCR5-expressing CD8⁺ T cells curtail chronic viral infection. *Nature* **537**, 412–428 (2016).
9. Jadhav, R. R. et al. Epigenetic signature of PD-1^{TCF1}CD8 T cells that act as resource cells during chronic viral infection and respond to PD-1 blockade. *Proc. Natl Acad. Sci. USA* **116**, 14113–14118 (2019).
10. Zander, R. et al. CD4⁺ T cell help is required for the formation of a cytolytic CD8⁺ T cell subset that protects against chronic infection and cancer. *Immunity* **51**, 1028–1042 (2019).
11. Hudson, W. H. et al. Proliferating transitory T cells with an effector-like transcriptional signature emerge from PD-1⁺ stem-like CD8⁺ T cells during chronic infection. *Immunity* **51**, 1043–1058 (2019).
12. Sade-Feldman, M. et al. Defining T cell states associated with response to checkpoint immunotherapy in melanoma. *Cell* **175**, 998–1013 (2018).
13. Brummelman, J. et al. High-dimensional single cell analysis identifies stem-like cytotoxic CD8⁺ T cells infiltrating human tumors. *J. Exp. Med.* **215**, 2520–2535 (2018).
14. Jansen, C. S. et al. An intra-tumoral niche maintains and differentiates stem-like CD8 T cells. *Nature* **576**, 465–470 (2019).
15. Mann, T. H. & Kaeck, S. M. Tick-TOX, it's time for T cell exhaustion. *Nat. Immunol.* **20**, 1092–1094 (2019).
16. Bhatt, K. H. et al. Profiling HPV-16-specific T cell responses reveals broad antigen reactivities in oropharyngeal cancer patients. *J. Exp. Med.* **217**, e20200389 (2020).
17. Krishna, S. et al. Human papilloma virus specific immunogenicity and dysfunction of CD8⁺ T cells in head and neck cancer. *Cancer Res.* **78**, 6159–6170 (2018).
18. Bobisse, S. et al. Sensitive and frequent identification of high avidity neo-epitope specific CD8⁺ T cells in immunotherapy-naïve ovarian cancer. *Nat. Commun.* **9**, 1092 (2018).
19. Wieland, A. et al. T cell receptor sequencing of activated CD8 T cells in the blood identifies tumor-infiltrating clones that expand after PD-1 therapy and radiation in a melanoma patient. *Cancer Immunol. Immunother.* **67**, 1767–1776 (2018).
20. Simoni, Y. et al. Bystander CD8⁺ T cells are abundant and phenotypically distinct in human tumour infiltrates. *Nature* **557**, 575–579 (2018).
21. Rosato, P. C. et al. Virus-specific memory T cells populate tumors and can be repurposed for tumor immunotherapy. *Nat. Commun.* **10**, 567 (2019).
22. Gattinoni, L. et al. A human memory T cell subset with stem cell-like properties. *Nat. Med.* **17**, 1290–1297 (2011).
23. Kamphorst, A. O. et al. Rescue of exhausted CD8 T cells by PD-1-targeted therapies is CD28-dependent. *Science* **355**, 1423–1427 (2017).
24. Patel, J. J., Levy, D. A., Nguyen, S. A., Knochelmann, H. M. & Day, T. A. Impact of PD-L1 expression and human papillomavirus status in anti-PD1/PDL1 immunotherapy for head and neck squamous cell carcinoma—systematic review and meta-analysis. *Head Neck* **42**, 774–786 (2020).
25. Skeate, J. G., Woodham, A. W., Einstein, M. H., Da Silva, D. M. & Kast, W. M. Current therapeutic vaccination and immunotherapy strategies for HPV-related diseases. *Hum. Vaccines Immunother.* **12**, 1418–1429 (2016).
26. Ha, S. J. et al. Enhancing therapeutic vaccination by blocking PD-1-mediated inhibitory signals during chronic infection. *J. Exp. Med.* **205**, 543–555 (2008).
27. de Martel, C., Georges, D., Bray, F., Ferlay, J. & Clifford, G. M. Global burden of cancer attributable to infections in 2018: a worldwide incidence analysis. *Lancet Glob. Health* **8**, e180–e190 (2020).
28. Wieland, A. et al. Defining HPV-specific B cell responses in patients with head and neck cancer. *Nature*, <https://doi.org/10.1038/s41586-020-2931-3> (2020).

Publisher's note Springer Nature remains neutral with regard to jurisdictional claims in published maps and institutional affiliations.

© The Author(s), under exclusive licence to Springer Nature Limited 2021

Methods

Data reporting

No statistical methods were used to predetermine sample size. The experiments were not randomized and the investigators were not blinded to allocation during experiments and outcome assessment.

Patients, isolation of TILs and HLA-typing

Untreated patients with stage I HPV-positive HNSCC were enrolled at Emory University Hospital between March 2017 and April 2019 in accordance with an approved Emory University Institutional Review Board protocol (WINSHIP4008-17), with all patients providing informed consent. Samples from primary tumour, metastatic lymph nodes and peripheral blood were obtained at the time of surgery. TILs and PBMCs were isolated as described previously²⁸ and cryopreserved. DNA from whole blood or PBMCs was isolated using the Qiagen DNeasy Blood & Tissue kit and HLA class I loci were genotyped using a sequence-base typing method.

Multiplex immunohistochemistry

Seven-colour multiplex immunohistochemistry was performed with the OPAL Polaris system (Akoya Biosciences). Four-to-five-micrometre sections of formalin-fixed paraffin-embedded tumours from the patients with HNSCC were deparaffinized, hydrated and stained manually with anti-CD3 (clone F7.2.38, Dako), CD8 (clone C8/144B, eBiosciences), CD20 (clone L26, Invitrogen), TCF-1 (clone C63D9, Cell Signaling Technologies (CST)), PD-1 (clone D4W2J, CST) and cytokeratin (clone AE1/3, Dako) antibodies. Heat induced epitope retrieval (HIER) in EDTA (pH 9) or citrate (pH 6) buffer was performed before blocking non-specific binding and staining the tissues with the primary antibodies. The sections were sequentially stained with each primary, HRP-conjugated secondary antibody, tyramide signal amplification, and OPAL fluorophore according to the manufacturer's instructions. OPAL 480, 520, 570, 620, 690 and 780 dyes were used. The sections were counterstained with spectral DAPI (Akoya Biosciences). The stained slides were imaged and scanned using the Vectra Polaris multispectral imaging system.

Image analysis

Random tumour areas (that included tumour parenchyma and stroma) of high-resolution whole-slide scanned images were first annotated in PhenoChart 1.0.12 (Akoya Biosciences) and then analysed with the inForm2.4.8 software (Akoya Biosciences). Tumour parenchyma and stroma areas were identified using DAPI and cytokeratin as a marker for the tumour parenchyma. Adaptive cell segmentation was accomplished on the basis of nuclear DAPI and membranous CD8. At least 30 cells from the phenotypes of the immune cells of interest were manually selected and used to train the software for automated phenotyping. Five to six representative regions per tumour sample were analysed for a total area of 3.2 to 3.8 mm² per tumour. The data were processed in R studio using phenoptr (v.0.2.5) and phenoptrReports (v.0.2.6) (Akoya Biosciences).

Flow cytometry

Cryopreserved PBMCs and TILs were thawed, counted and stained in Dulbecco's phosphate buffered saline (DPBS) + 2% FBS with LIVE/DEAD Fixable Yellow or Aqua Dead Cell Stain Kit (1:200, Life Technologies) and surface-stain antibodies at 0.5 tests per 1 × 10⁶ cells in brilliant stain buffer (BD Bioscience, 563794; for antibodies see Supplementary Table 1). For tetramer stain, tetramers were generated from monomers according to standard protocol²⁹ and stored at -20 °C in 50% glycerol. Cells were incubated for 10 min at room temperature with the tetramers at 1:100 in DPBS, followed by addition of extracellular staining antibodies for 25 min. Cells were fixed and permeabilized with a Fixation/Permeabilization Kit (Invitrogen, 00-8333-56) or BD Cytotfix/Perm Kit (BD, 554714) for ICCS, followed by intracellular staining (for antibodies see Supplementary Table 1). All data were acquired the same day on an LSR II cytometer, FACS Canto II or FACSymphony A5 with FACSDiva

v.8.0.1 (BD Biosciences) and analysed using FlowJo software (v.10.6.1, Tree Star; for gating strategy see Extended Data Fig. 10a, b).

HPV-specific T cell expansion

PBMCs and TILs from 17 patients with HPV-positive HNSCC were used for in vitro T cell expansion. Potential CD8 T cell epitopes derived from HPV proteins E2, E5, E6 and E7 and presented by a reference set of 27 human leukocyte antigens (HLA-A, B and C) covering 97% of the population were predicted using the Immune Epitope Database (IEDB)³⁰. A total of 251 predicted 9–10-amino-acid-long peptides with a percentile rank of less than or equal to 1 (Supplementary Table 2) were synthesized as crude material (A&A Labs) and ultimately resuspended in DMSO. A peptide pool was prepared containing all 251 peptides from proteins E2 (125 peptides), E5 (55 peptides), E6 (50 peptides) and E7 (21 peptides). PBMCs were cultured in complete CTS OpTmizer medium (CTS OpTmizer T Cell Expansion SFM with CTS supplement A1048501, substituted with L-glutamine, penicillin–streptomycin and 2% human serum, Sigma-Aldrich, H3667) in the presence of the HPV-peptide pool (1 µg ml⁻¹ per peptide), rIL-2 (Peprotech, 50 IU ml⁻¹), rIL-7 (Peprotech, 25 ng ml⁻¹) and rIL-15 (Peprotech, 25 ng ml⁻¹). HPV-peptides were only added on the first day of culture, whereas cytokines were supplemented whenever cells were split during the two-week expansion period. At day 13 of cell culture, expanded cells were washed and rested overnight in cytokine-free medium.

Identification of epitopes by ELISpot and ICCS

Expanded and rested cells were plated in an IFNγ ELISpot (1 × 10⁵ cells per well, BD Elispot Human IFNγ ELISPOT, 551873, IP Sterile White plates 0.45 µm hydrophobic high protein binding, Merck Millipore, S2EM004M99) and stimulated overnight with 32 different megapools containing up to 16 of the predicted peptides, with each peptide being represented in 2 megapools (2 µg ml⁻¹ per peptide). If the two megapools were positive, the potential positive peptide (1 µg ml⁻¹) was used individually to stimulate rested expanded cells in an IFNγ ELISpot. Peptides scoring positive were further confirmed to be recognized by CD8 T cells using ICCS. Cryopreserved expanded cells were thawed, rested overnight and simulated with the candidate peptide (10 µg ml⁻¹) in the presence of brefeldin A and monensin (BD Golgi-Plug, 555029, and BD Golgi-Stop, 554724, 1:1,000). After 6 h, cells were washed with PBS + 2% FBS and stained for flow cytometric analysis as detailed above. For each recognized peptide sequence, the binding affinity to the responder's HLA class I alleles was predicted in silico (<http://www.iedb.org/>). The HLA class I allele with the highest binding affinity for each epitope was retained as a HLA–peptide pair.

Generation of HPV-specific tetramers

Peptides of identified HLA–peptide pairs were synthesized at greater than 90% purity (A&A Labs) and the binding affinity to the respective HLA class I alleles was determined by in vitro binding assays³¹. Ten HLA–monomers were generated by the NIH Tetramer Core facility, one by ImmunaWare (HLA-A*29:02 E5_{65–73} (peptide sequence IFVYIPLFL)) and one in our laboratory (HLA-A*02:01-E5_{46–54} (peptide sequence VLLLWITAA)). Monomers were then tetramerized in house. Tetramer staining was tested on expanded PBMCs and frequencies of tetramer-positive CD8 T cells were similar to frequencies of IFNγ-positive CD8 T cells previously quantified by ICCS. We successfully produced the following HLA–tetramers: HLA-A*01:01–HPV E2_{151–159} (peptide sequence QVDYGLYY), HLA-A*01:01–HPV E2_{329–337} (peptide sequence KSAIVTLTY), HLA-A*02:01–HPV E5_{46–54} (peptide sequence VLLLWITAA), HLA-B*35:01–HPV E5_{55–63} (peptide sequence SAFRCFIVY), HLA-A*29:02–HPV E5_{65–73} (peptide sequence IFVYIPLFL), HLA-B*35:01–HPV E6_{52–61} (peptide sequence FAFRDLCIVY) and HLA-B*27:05–HPV E6_{83–90} (peptide sequence FAFRDLCIVY).

Sorting of HPV-positive CD8 T cells from lymphocytes infiltrating tumour and metastatic lymph nodes

Cryopreserved TILs from primary tumours or metastatic lymph nodes were thawed, rested for 3 h in RPMI + 10% FBS (R10, supplemented with

Article

1% penicillin, streptomycin and L-glutamine) at 37 °C, 5% CO₂ and stained with tetramer in two different colours, followed by surface marker staining as described above. Live CD3⁺CD19⁻CD14⁻CD16⁻CD4⁻CD8⁺ double-tetramer-positive cells (for gating strategy see Extended Data Fig. 10c) were sorted on an ARIA II (BD Bioscience) into PBS with 2% FBS. For patients for whom scRNA-seq was performed, we confirmed by PCR that epitopes were not mutated and that the DNA encoding the corresponding epitopes was detectable in the tumour tissue (data not shown).

Single-cell and TCR analysis

Alignment, filtering, barcode counting and unique molecular identifier counting were performed using Cell Ranger v.3.1. Data were further analysed using Seurat v.3.1.4³². All single-cell analysis was performed using R v.3.6.2. In brief, cells with a percentage of mitochondrial genes below 0.07% were included. Cells with more than 6,000 or fewer than 1,000 detected genes were considered as outliers and excluded from the downstream analyses. Samples from different patients were merged using the Seurat function FindIntegrationMarkers, which identifies and calculates anchors between pairs of datasets to reduce the sample batch effect. Principal component analysis was performed, and the top 6–8 most statistically significant principal components were used for uniform manifold approximation and projection (UMAP) analysis. Components enriched for cell-cycle genes were excluded from UMAP clustering. Marker genes that were differentially expressed within each cluster were identified by the Seurat function FindAllMarkers with average log-transformed fold change cut-offs of 0.5. Scaled expression data of the top 20 marker genes were used to create the heat maps. Gene set scoring was performed using the VISIONR package v.2.1.0, following the scoring algorithm as previously described³³. In brief, the expression of signature genes is weighted on the basis of predicted dropout probability calculated from nearest neighbours, and the normalized expression summed for all genes in the gene set. TCR analysis was performed using Cell Ranger. Unique clonotypes were defined by CDR3 alpha and beta sequences. Cells for which we failed to recover both alpha and beta chains were treated as unique clones, even if the recovered chain overlapped with another clonotype that had found both alpha and beta chains.

Pseudotime³⁴ was calculated using the Monocle3 v.0.2.3.0 package. In brief, we enforced a model in which cells started in the root node in the stem-like population. This assumption was based on extensive data in mice and humans indicating that this cell is the precursor of other T cell populations. We then calculated a trajectory that first passed through the transitional population and ended in a leaf node of the terminally differentiated population. These assumptions were based on the transitional population of cells expressing intermediate levels of many genes between the stem and terminally differentiated cells.

In vitro proliferation assay

Cryopreserved TILs from primary tumours or metastatic lymph nodes were thawed, rested for 3 h in RPMI + 10% FBS (R10, supplemented with 1% penicillin, streptomycin and L-glutamine) at 37 °C, 5% CO₂ and subsequently labelled with CTV, followed by staining of cell-surface markers (as described above). PD-1⁺CD45RA⁻CD8 T cells (live CD3⁺CD19⁻CD14⁻CD16⁻CD4⁻CD8⁺) were sorted on the basis of the expression of TIM-3 and CD39 on an ARIA II (BD Bioscience) into PBS with 2% FBS, with stem-like cells being TIM-3⁻CD39⁻ and terminally differentiated cells being TIM-3⁺CD39⁺ (for gating strategy see Extended Data Fig. 9a). Sorted cell populations were cultured alone or with patient-matched, irradiated (20 Gy) PBMCs pulsed with 10 µg ml⁻¹ peptide for 5 days in R10 with 20–50 U ml⁻¹ rIL-2 at 37 °C, 5% CO₂, followed by staining for flow cytometric analysis.

Statistical analysis

Data are presented as mean ± s.d. Paired two-tailed *t*-tests and Wilcoxon matched-pairs rank tests were used when appropriate and as indicated,

with **P* < 0.05, ***P* < 0.01, ****P* < 0.001 and *****P* < 0.0001. All statistical analyses were performed using GraphPad Prism v.8.3.

Reporting summary

Further information on research design is available in the Nature Research Reporting Summary linked to this paper.

Data availability

The following protein sequences were used for predicting and generating HPV peptides: E2 (Uniprot P03120), E5 (Uniprot P06927), E6 (Uniprot P03126), and E7 (Uniprot P03129). scRNA-seq data are available in the NCBI Gene Expression Omnibus (GEO) database under the accession number GSE180268. Other relevant data are available from the corresponding authors upon reasonable request.

Code availability

Custom code for scRNA-seq is available from the corresponding authors upon reasonable request.

29. NIH Tetramer Core Facility. *Production Protocols: Class I MHC Tetramer Preparation* <https://tetramer.yerkes.emory.edu/support/protocols#10> (2006).
30. Vita, R. et al. The Immune Epitope Database (IEDB): 2018 update. *Nucleic Acids Res.* **47**, D339–D343 (2019).
31. Sidney, J. et al. Measurement of MHC/peptide interactions by gel filtration or monoclonal antibody capture. *Current Protoc. Immunol.* **100**, 18.3.1–18.3.36 (2013).
32. Satija, R., Farrell, J. A., Gennert, D., Schier, A. F. & Regev, A. Spatial reconstruction of single-cell gene expression data. *Nat. Biotechnol.* **33**, 495–502 (2015).
33. DeTomaso, D. & Yosef, N. FastProject: a tool for low-dimensional analysis of single-cell RNA-seq data. *BMC Bioinformatics* **17**, 315 (2016).
34. Trapnell, C. et al. The dynamics and regulators of cell fate decisions are revealed by pseudotemporal ordering of single cells. *Nat. Biotechnol.* **32**, 381–386 (2014).

Acknowledgements This work was supported by funding from the Ambrose Monell Foundation (R.A.); the T. J. Martell Foundation (R.A.); NIH grants 5U19AI057266 and P01AI056299 (R.A.); the Oliver S. and Jennie R. Donaldson Charitable Trust (R.A.); a Winship Invest \$ Pilot grant (R.A., Z.G.C. and N.F.S.); Swiss National Science Foundation grant P300PB_174483 (C.S.E.); a Eugenio Litta Foundation grant (C.S.E.); NCI grant 1-R00-CA197891 (H.T.K.); the James M. Cox Foundation and James C. Kennedy (H.T.K.); the Prostate Cancer Foundation (H.T.K. and N.P.); and a Triological Society Research Career Development Award (M.R.P.). We thank H. Wu for technical assistance and M. Clayton for administrative support. We acknowledge the Emory Flow Cytometry Core supported by the National Center for Georgia Clinical and Translational Science Alliance of the NIH under award number UL1TR002378; the Integrated Cellular Imaging Microscopy Core of the Winship Cancer Institute of Emory University and the NIH–NCI under award number, 2P30CA138292-04; and the Yerkes NHP Genomics Core, which is supported in part by NIH P51 OD011132. This research was supported in part by the Intramural Research Program of the NIH, the Frederick National Laboratory for Cancer Research and the Center for Cancer Research. The project has been funded in part with federal funds from the Frederick National Laboratory for Cancer Research, under contract no. HHSN261200800001E. The content of this publication does not necessarily reflect the views or policies of the Department of Health and Human Services, nor does mention of trade names, commercial products or organizations imply endorsement by the US Government.

Author contributions C.S.E. performed most of the experiments and analysed the data. H.T.K. analysed the scRNA-seq data. M.R.P. collected and provided human specimens, and analysed patient data. M.A.C. analysed scRNA-seq data. M.A.C., N.P. and A.W. performed in vitro proliferation experiments. R.C.O. performed and analysed multiplex immunohistochemistry experiments. T.H.N. performed flow cytometry experiments. C.C.G. and X.W., supervised by D.M.S., handled human specimens. M.C. performed HLA-typing analyses. J.S. and A.S. performed peptide–MHC affinity measurements. D.M.S., N.F.S. and Z.G.C. initiated the clinical specimen protocol. A.W. processed human specimens. A.W. and R.A. conceived, designed and supervised the project, and contributed equally to this work. C.S.E., H.T.K., A.W. and R.A. wrote the manuscript, with all authors contributing to the revision of the manuscript.

Competing interests R.A. holds patents related to the PD-1 inhibitory pathway. C.S.E., A.W. and R.A. are inventors on a patent application filed by Emory University relating to the use of HPV-specific TCR sequences. All other authors declare no competing interests.

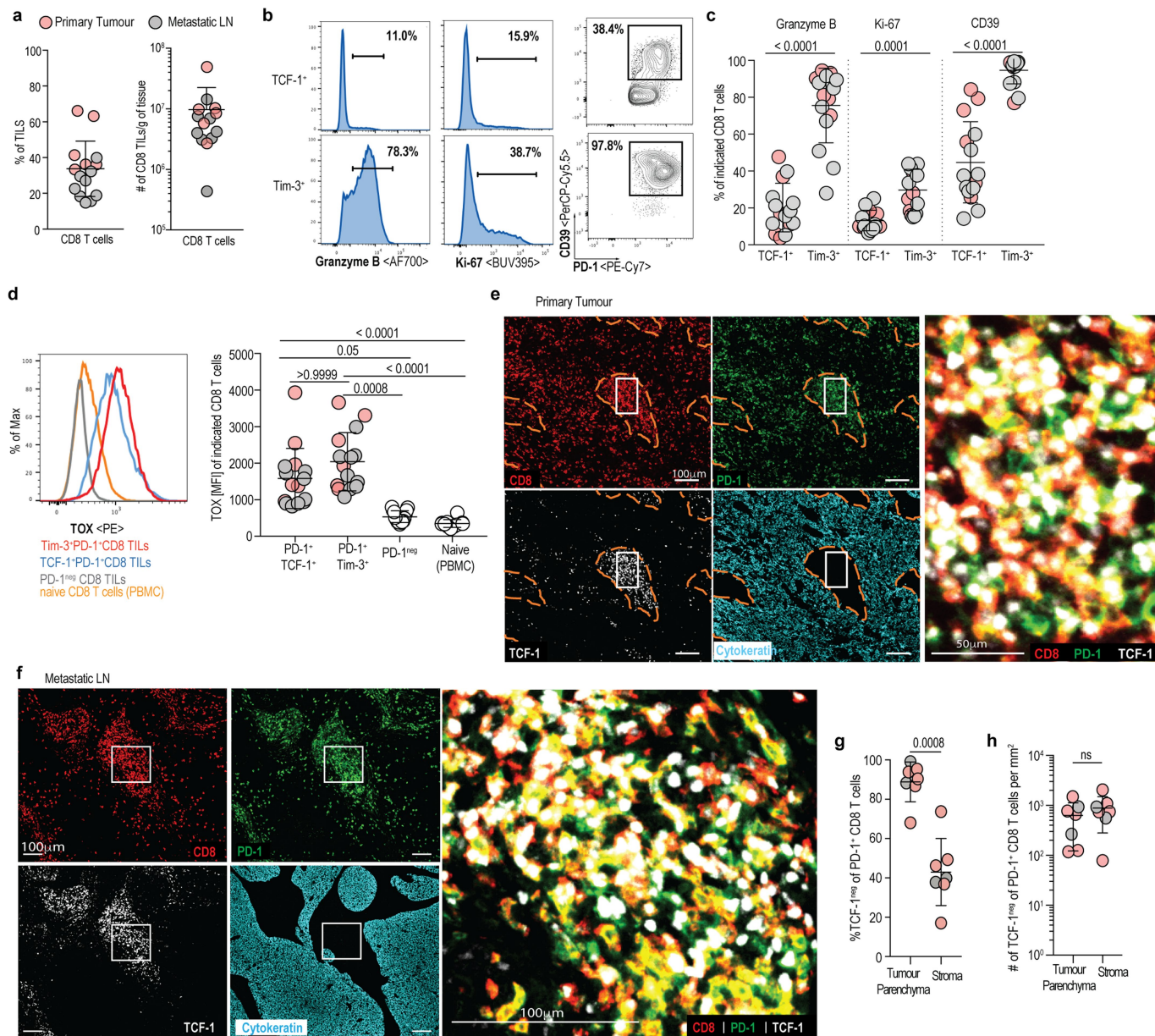
Additional information

Supplementary information The online version contains supplementary material available at <https://doi.org/10.1038/s41586-021-03862-z>.

Correspondence and requests for materials should be addressed to A.W. or R.A.

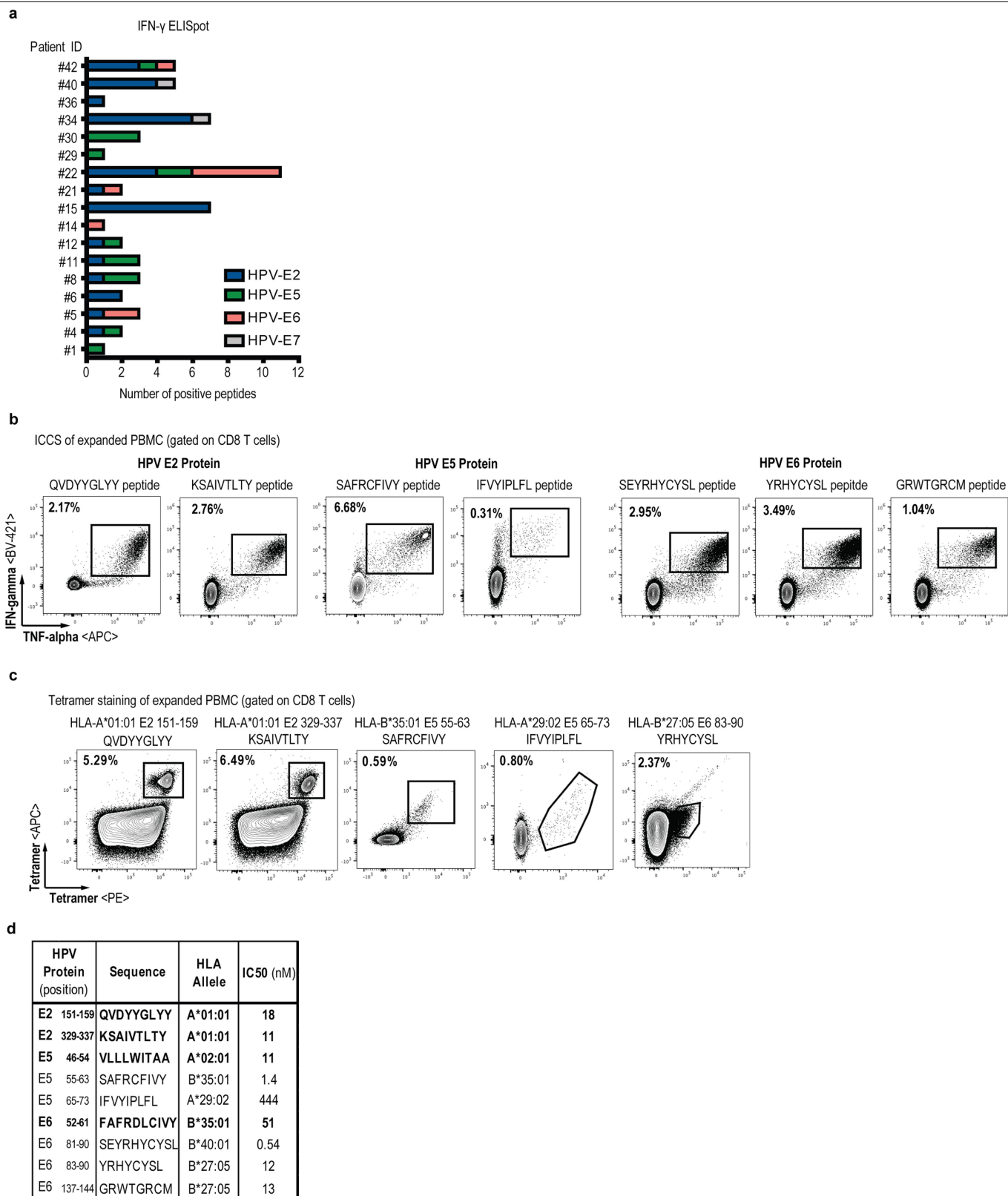
Peer review information Nature thanks Benny Chain, Evan Newell and the other, anonymous, reviewer(s) for their contribution to the peer review of this work.

Reprints and permissions information is available at <http://www.nature.com/reprints>.



Extended Data Fig. 1 | Analysis of PD-1⁺ CD8 TILs in patients with HPV-positive HNSCC. **a**, Frequency of CD8 T cells among TILs and number of CD8⁺ TILs per gram of HPV-positive HNSCC primary tumours (pink) and metastatic lymph nodes (metLN, grey), with mean and SD. **b**, Representative flow plots showing Granzyme B, Ki-67, and CD39 expression among TCF-1⁻Tim-3⁻ and Tim-3⁺TCF-1⁻ CD8 T cell subsets in TILs. **c**, Frequency of Granzyme B⁺, Ki-67⁺ and CD39⁺ cells among PD-1⁺ CD8 TIL subsets, with means and SD. Two-sided Wilcoxon matched-pairs rank test. **d**, Geometric mean fluorescence intensity (MFI) of TOX in CD8 TIL subsets and patient-matched naive peripheral blood CD8 T cells (CD3⁺CD4⁺CD8⁺CCR7⁺CD45RA⁺), with means and SD. Friedman test with two-sided Dunn's multiple comparisons test. **e, f**, Multiplex immunohistochemistry of primary tumour (**e**) and (**f**) metastatic lymph nodes

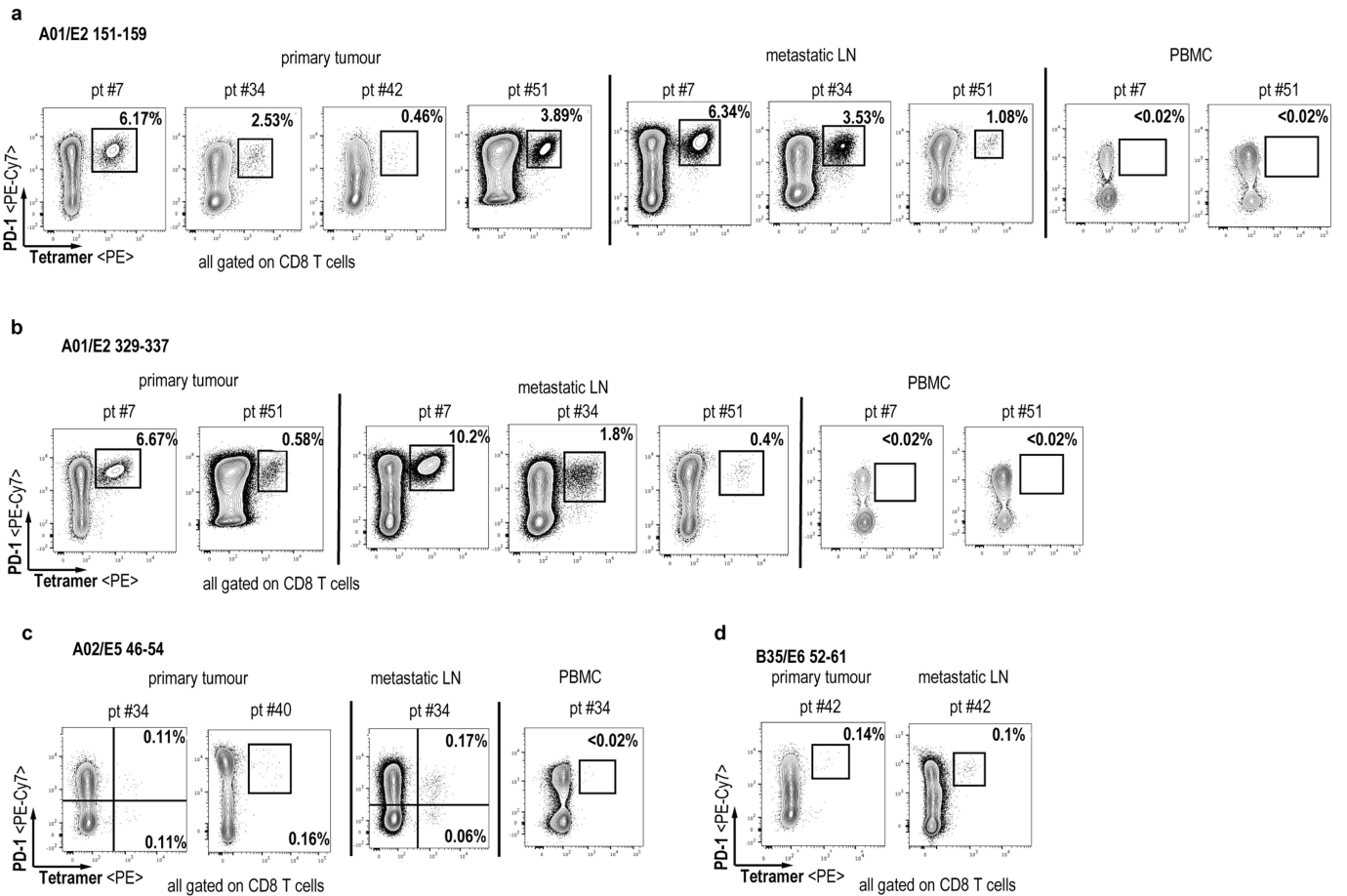
(metLN) showing CD8⁺ (red) and PD-1⁺ (green) cells infiltrating the tumour parenchyma (cytokeratin⁺; blue) and stroma (cytokeratin negative; black areas highlighted by the orange dashed lines). TCF-1⁺ cells (white) are predominantly found in the stromal regions of the metastasis. Composite image on the right shows stem-like CD8 T cells (CD8⁺PD-1⁺TCF-1⁻; yellow membranous staining with white nuclear marker) within the stroma at a higher magnification of the area corresponding to the white rectangle. **g, h**, Frequency (**g**) and density (**h**) of PD-1⁺TCF-1⁻ CD8 TILs in the tumour parenchyma and stroma, with mean and SD. *n* = 7 (five primary tumours (pink) and two metastatic lymph nodes (grey)). ns = not significant, two-sided paired t-tests.



Extended Data Fig. 2 | Mapping of HPV-specific CD8⁺ T cell epitopes in patients with HNSCC. a. Summary graph showing the numbers of positive peptides from HPV E2 (blue), E5 (green), E6 (red) and E7 (grey) proteins in expanded T cells of patients with HPV-positive HNSCC ($n = 17$) as measured by IFN γ ELISpot. **b.** Flow plots of expanded PBMC re-stimulated with the identified

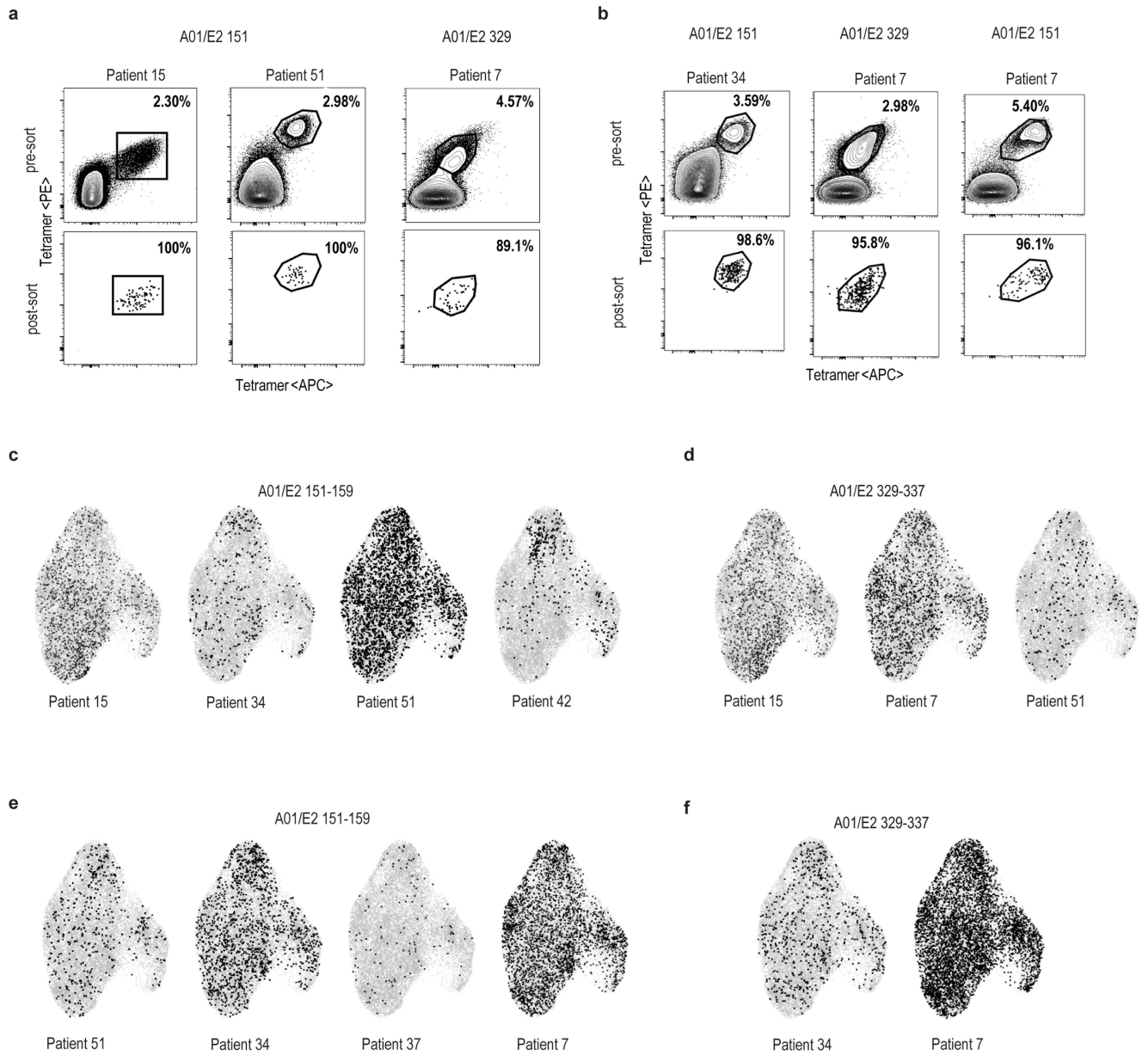
peptides and analysed by ICCS for IFN γ and TNF α . Gated on CD3⁺CD4⁻CD8⁺ cells. **c.** Flow plots of expanded PBMC stained with HPV-specific MHC-I tetramers. Gated on CD3⁺CD4⁻CD8⁺ cells. **d.** Table summarizing results of the HLA-binding assays (IC₅₀) of identified HPV epitopes. Indicated in bold are epitopes for which ex vivo tetramer staining was performed.

Direct ex vivo staining of TILs and PBMC



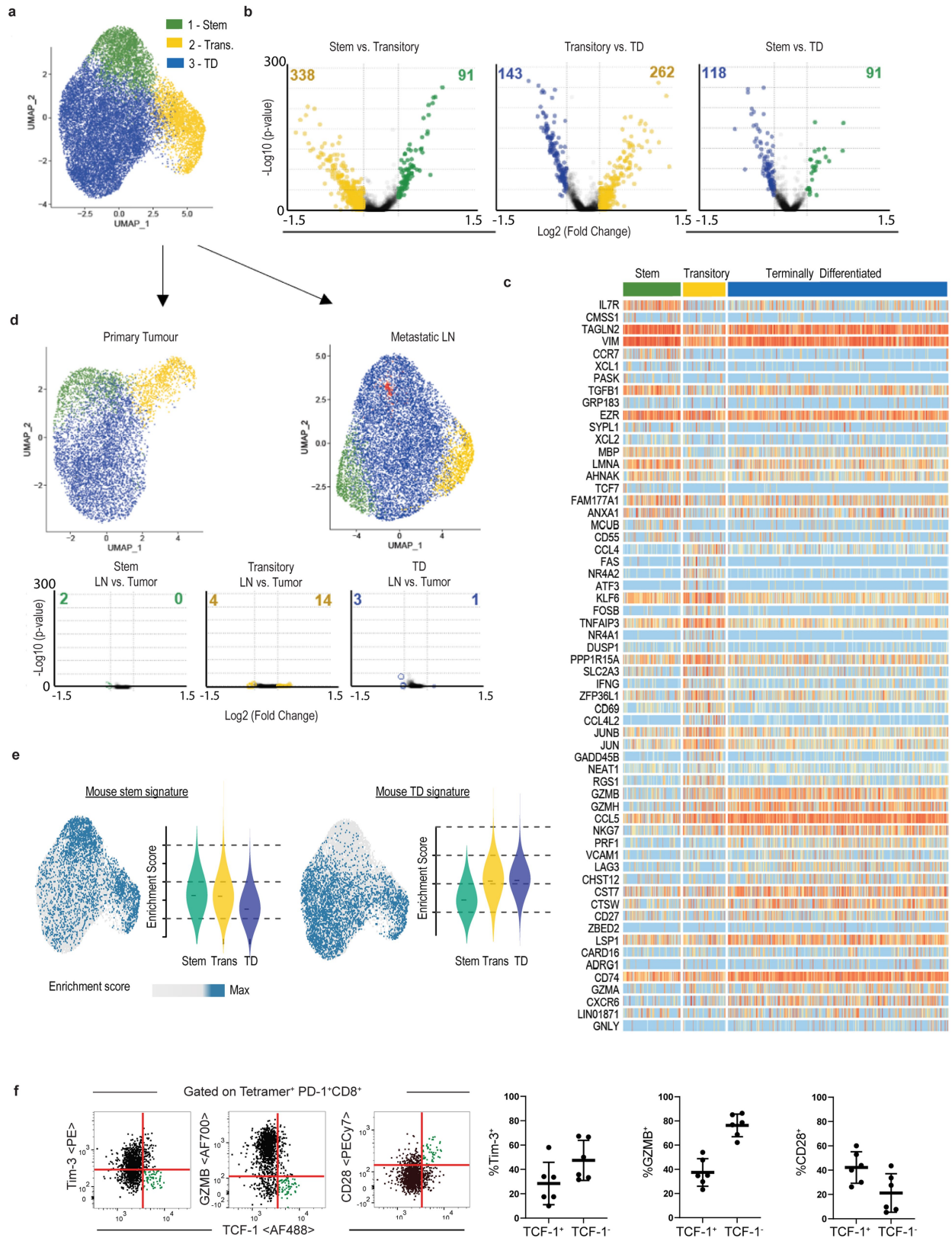
Extended Data Fig. 3 | Direct ex vivo tetramer staining of TILs and PBMCs from patients with HNSCC. TILs from primary tumours and metastatic lymph nodes as well as matched PBMC samples were tetramer-stained ex vivo with HPV-specific tetramers. Flow plots showing tetramer⁺ CD8 T cells in primary

tumours, metastatic LN and PBMC. The cells were stained with the following tetramers: **a**, A01/E2151-159, **b**, A01/E2329-337, **c**, A02/E5 46-54 and **d**, B35/E6 52-61. Gated on CD3⁺CD4⁻CD8⁺ cells.



Extended Data Fig. 4 | MHC-I tetramer sorting and scRNA-seq analysis of HPV-specific PD-1⁺ CD8 T cells from primary tumour and metastatic lymph nodes. a, b. Flow cytometry plots showing pre- and post-sorted tetramer-positive cells from primary and metastatic tumours. **c–f.** scRNA-seq

data of the 13 tetramer-sorted samples showing the relative distribution among the three different clusters (stem-like, transitory and exhausted) in HPV-specific CD8 T cells in each sample.

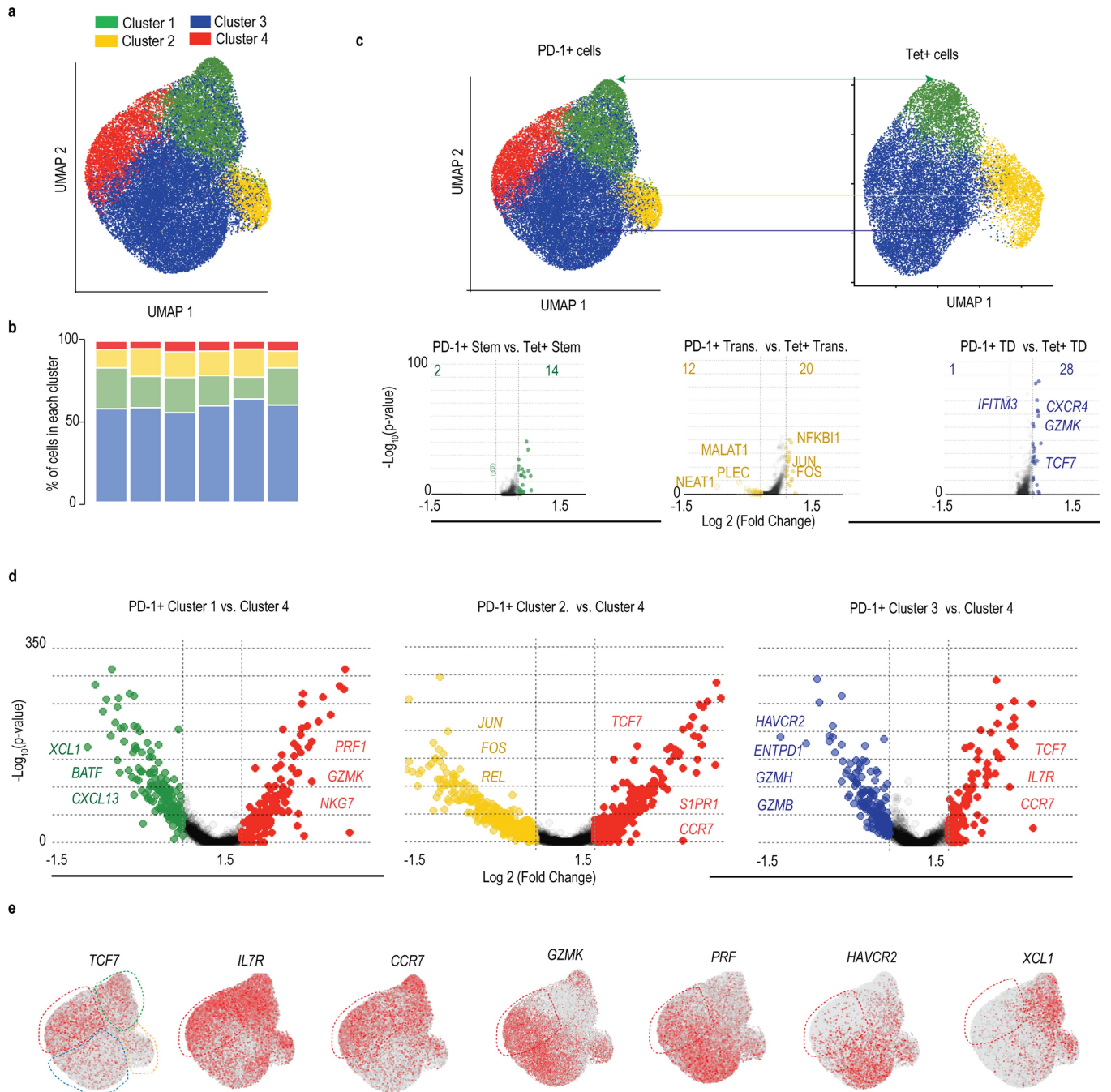


Extended Data Fig. 5 | See next page for caption.

Article

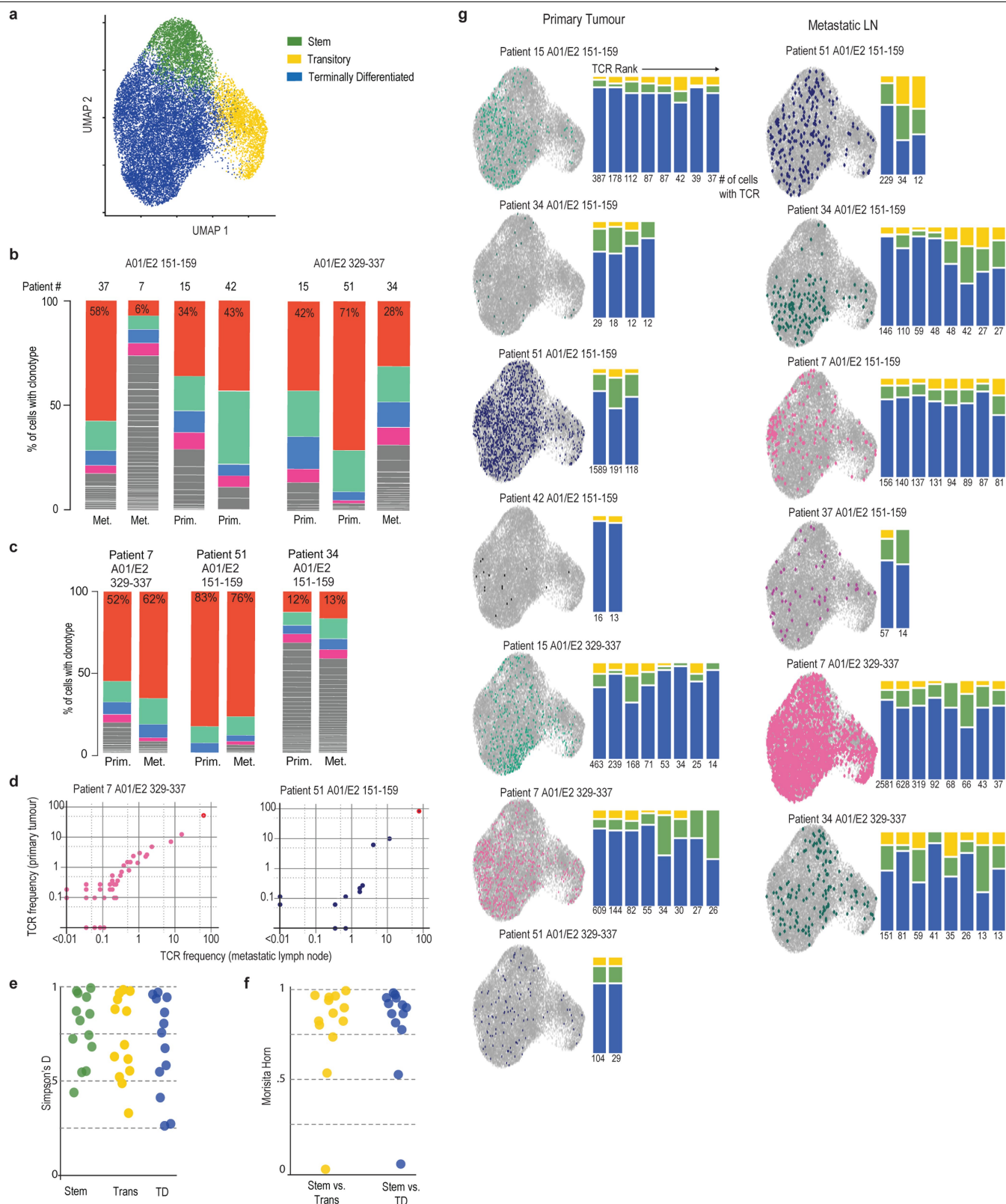
Extended Data Fig. 5 | Comparison of HPV-specific PD-1⁺ CD8 T cells in primary tumour and metastatic lymph nodes. HPV tetramer-specific CD8 T cells from 13 samples including seven primary tumours and six metastatic lymph nodes were sorted and subjected to single cell RNAseq. **a**, UMAP clustering of HPV tetramer-specific CD8 T cells combined from all 13 samples, irrespective of tumour site, identified three distinct clusters; #1 stem-like, #2 transitory and #3 terminally differentiated/exhausted. **b**, Pairwise comparison of identified clusters among all HPV tetramer-specific CD8 T cells. Volcano plots show average fold-change by all cells in the cluster by $-\log_{10}$ p-value. The number of differentially expressed genes ($\geq 0.25 \text{ Log}_2$ fold-change in each pairwise comparison) are indicated in each plot. **c**, Heat map showing the top differentially expressed genes. The top 25 most significant genes from each cluster are shown. **d**, To assess gene expression differences of HPV-specific CD8 T cells in the two sites, we performed UMAP clustering of cells isolated from primary tumour and metastatic lymph node samples, respectively. We

identified three clusters in primary tumours and four in metastatic lymph nodes. Gene expression was compared between the respective subsets (Green \rightarrow Green; Yellow \rightarrow Yellow; Blue \rightarrow Blue) in each tissue. Volcano plots highlight the differences between these clusters. The orange cluster identified in the metastatic lymph nodes consisted of very few cells and was thus not included in the comparisons. **e**, VISION analysis of HPV-specific CD8 T cells for enrichment of gene signatures associated with LCMV-specific stem-like and terminally differentiated/exhausted CD8 T cells. UMAP plots show the top quintile of cells enriched for the signature in blue. **f**, FACS analysis of various markers for HPV tetramer-specific intratumoral CD8 T cells. Plots are gated on PD-1⁺ HPV-specific CD8 T cells and show the respective marker versus TCF-1, the defining transcription factor of stem-like CD8 T cells. Summary plots show the frequency of TCF-1⁺ and TCF-1⁻ cells expressing the respective marker for six patient samples.



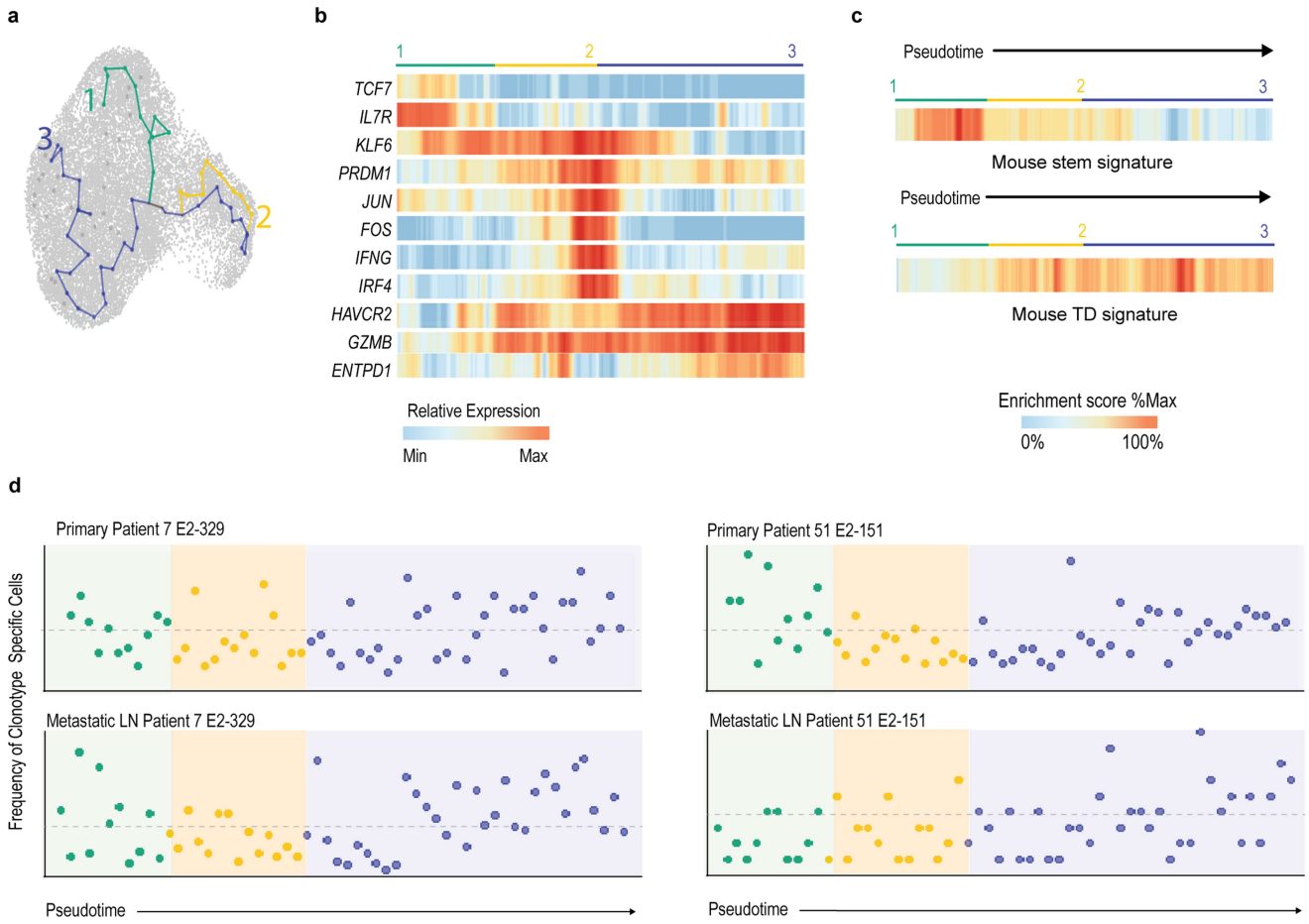
Extended Data Fig. 6 | Comparing the transcriptional program of total PD-1⁺ CD8 T cells with HPV-specific PD-1⁺ CD8 T cells in the tumour. To compare total PD-1⁺ CD8 T cells with HPV-specific PD-1⁺ CD8 T cells in the TME, we performed scRNA-seq of total PD-1⁺ CD8 T cells (depleted of identified HPV-specific CD8 T cell reactivities) and used analysis techniques similar to those in Fig. 3. **a**, UMAP clustering of PD-1⁺ CD8 T cells. Cells from six samples (three patients, primary tumour and metastatic lymph nodes) were computationally combined, and four distinct clusters were identified. **b**, Distribution of individual samples among the four identified clusters. **c**, Comparison of gene expression differences between total PD-1⁺ CD8 T cells

and HPV tetramer-positive CD8 T cells. The corresponding clusters of cells from HPV tetramer-specific CD8 T cells were compared to the cells found among total PD-1⁺ CD8 T cells. Clusters 1-3 mapped very closely to what was found in the HPV-specific cells, with relatively few differentially expressed genes. **d**, Comparison of cluster 4 in PD-1⁺ cells to clusters of HPV-specific cells. Cluster 4 was compared to the other clusters to identify specific gene differences. Volcano plots show fold change versus $-\log(p\text{-value})$ for each gene. **e**, UMAP plots show selected genes that are significantly up- or down-regulated in this cluster versus others from the PD-1⁺ cells.



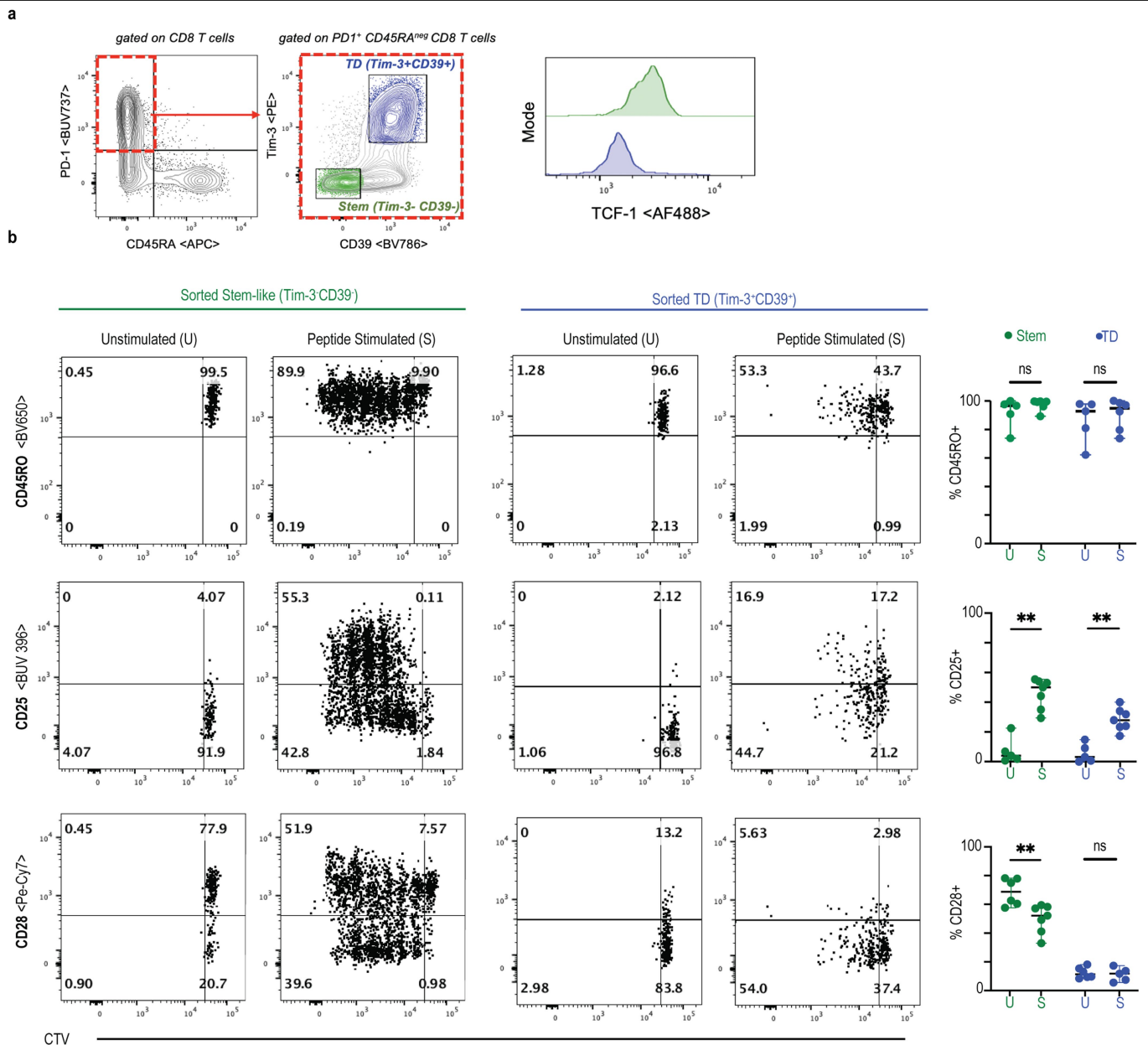
Extended Data Fig. 7 | HPV-specific CD8 T cell clonotypes exist in multiple differentiation states. **a**, UMAP clustering of HPV tetramer-specific CD8 T cells. **b**, TCR repertoire of tetramer-positive CD8 TILs in primary tumours (Prim.) and metastatic lymph nodes (Met.) with the top four clonotypes highlighted. Colours do not indicate the same clonotype between patients or epitope reactivities. **c**, TCR repertoire of tetramer-positive CD8 TILs in matched primary tumour and metastatic lymph node of the same patient with the top 4 clonotypes highlighted. Colours indicate the same clonotype within a patient and epitope reactivity. **d**, TCR frequency in patients with matched

primary and metastatic tissue. **e**, TCR diversity of the identified clusters. **f**, Overlap between clusters for each patient as determined by Morisita Horn index. **g**, Distribution of the most frequent TCR clonotypes for each patient and epitope across gene expression clusters. UMAP plots show the distribution of the most frequent TCR clonotype across clusters. Accompanying bar charts showing the distribution of the eight most prominent TCR clonotypes across all clusters (clonotypes with less than 10 cells are not shown). The number of cells of the respective TCR clonotype is indicated below.



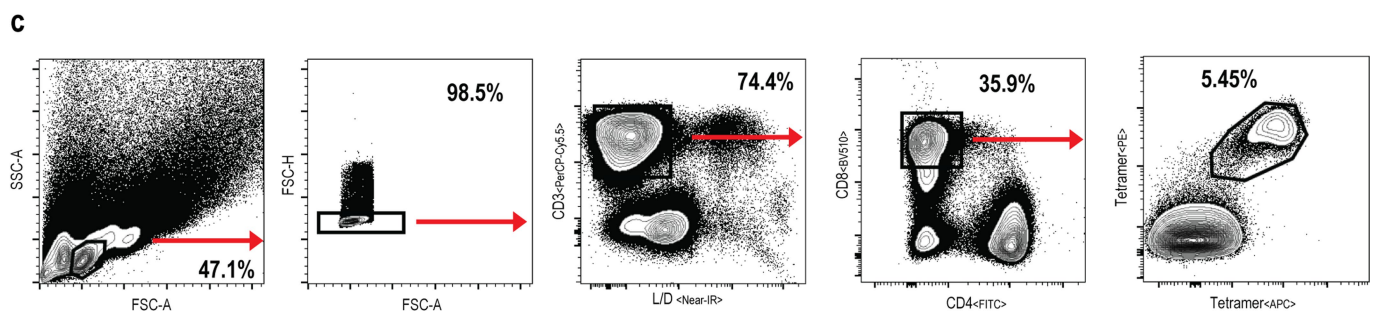
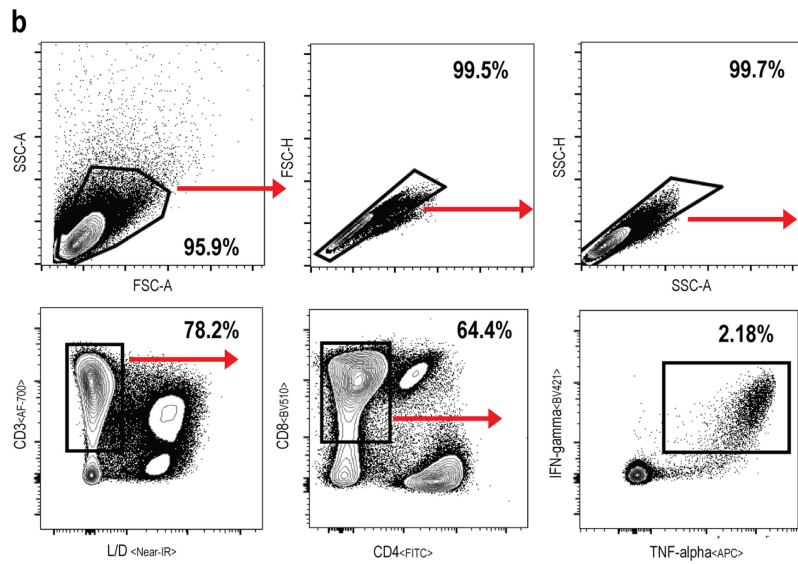
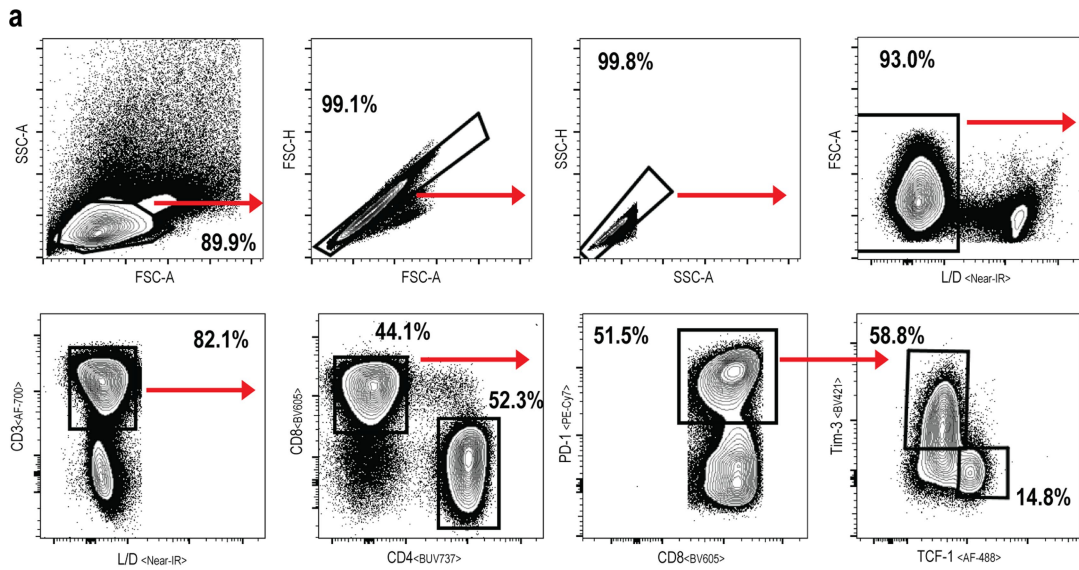
Extended Data Fig. 8 | Pseudotime analysis to investigate the lineage relationship of HPV-specific PD-1⁺ CD8 T cell subsets. **a–c**, Pseudotime analysis of HPV tetramer-positive CD8 T cells showing a differentiation trajectory where cells start as stem-like PD-1⁺TCF-1⁺ cells, transition through an intermediate stage, before taking on a terminally differentiated state. Selected

genes (**b**) and enrichments for stem- and terminally differentiated gene signatures (**c**) are shown through this trajectory. **d**, Pseudotime analysis showing the distribution of the immunodominant clonotype of patients 7 and 51 in primary tumour and metastatic site through pseudotime.



Extended Data Fig. 9 | Proliferation and differentiation potential of HPV-specific stem-like CD8 T cells. **a**, Flow plots showing the gating strategy to isolate stem-like (CD39⁻Tim-3⁻) and terminally differentiated cells (CD39⁺Tim-3⁺) PD-1⁺CD45RA^{high} CD8 T cells. Histograms showing TCF-1 expression to validate that the sorting strategy using CD39 and Tim-3 as surrogate markers enriches for stem-like (green) and terminally differentiated

(blue) cells. **b**, Representative plots showing CTV dilution and expression of CD45RO, CD25 and CD28 after five days of culturing stem-like and terminally differentiated CD8 T cells alone or with peptide-pulsed PBMCs. Summary plots show percentage of cells positive for the indicated markers on day five. Means and their SD are represented, ** < 0.01, ns = not significant, unpaired Mann-Whitney U test.



Extended Data Fig. 10 | Gating strategies. a, Flow plots showing the gating strategy for bulk TIL staining and gating on live CD3⁺CD8⁺PD-1⁻ (shown in Fig. 1a) and Tim-3/TCF-1⁺ cells (shown in Fig. 1b-d). **b**, Flow plots showing the gating strategy for ICCS of expanded T cells measuring IFN γ and TNF α

expression of live CD3⁺CD4⁻CD8⁺ cells (shown in Fig. 2b). **c**, Flow plots showing the sort gating strategy for ex vivo TIL staining (shown in Fig. 2c). Tetramer-positive CD8 T cells were gated as live CD3⁺CD4⁻CD8⁺ double-tetramer⁺ cells.

Reporting Summary

Nature Research wishes to improve the reproducibility of the work that we publish. This form provides structure for consistency and transparency in reporting. For further information on Nature Research policies, see [Authors & Referees](#) and the [Editorial Policy Checklist](#).

Statistics

For all statistical analyses, confirm that the following items are present in the figure legend, table legend, main text, or Methods section.

- | n/a | Confirmed |
|-------------------------------------|--|
| <input type="checkbox"/> | <input checked="" type="checkbox"/> The exact sample size (n) for each experimental group/condition, given as a discrete number and unit of measurement |
| <input type="checkbox"/> | <input checked="" type="checkbox"/> A statement on whether measurements were taken from distinct samples or whether the same sample was measured repeatedly |
| <input type="checkbox"/> | <input checked="" type="checkbox"/> The statistical test(s) used AND whether they are one- or two-sided
<i>Only common tests should be described solely by name; describe more complex techniques in the Methods section.</i> |
| <input checked="" type="checkbox"/> | <input type="checkbox"/> A description of all covariates tested |
| <input checked="" type="checkbox"/> | <input type="checkbox"/> A description of any assumptions or corrections, such as tests of normality and adjustment for multiple comparisons |
| <input type="checkbox"/> | <input checked="" type="checkbox"/> A full description of the statistical parameters including central tendency (e.g. means) or other basic estimates (e.g. regression coefficient) AND variation (e.g. standard deviation) or associated estimates of uncertainty (e.g. confidence intervals) |
| <input type="checkbox"/> | <input checked="" type="checkbox"/> For null hypothesis testing, the test statistic (e.g. F , t , r) with confidence intervals, effect sizes, degrees of freedom and P value noted
<i>Give P values as exact values whenever suitable.</i> |
| <input checked="" type="checkbox"/> | <input type="checkbox"/> For Bayesian analysis, information on the choice of priors and Markov chain Monte Carlo settings |
| <input checked="" type="checkbox"/> | <input type="checkbox"/> For hierarchical and complex designs, identification of the appropriate level for tests and full reporting of outcomes |
| <input checked="" type="checkbox"/> | <input type="checkbox"/> Estimates of effect sizes (e.g. Cohen's d , Pearson's r), indicating how they were calculated |

Our web collection on [statistics for biologists](#) contains articles on many of the points above.

Software and code

Policy information about [availability of computer code](#)

Data collection FACS data was collected on a BD LSR II, FACS Canto II or a FACSymphony A5 (BD Biosciences) using BD FACSDiva V8.0.1. ELISPOT data was acquired using CTL Immunospot Reader. Multiplex IHC data was collected using the Vectra Polaris Imaging System.

Data analysis FACS data was analysed with FlowJo V10.6.1. GraphPad Prism V7.0 was used for statistical analyses. scRNA-seq analyses were performed using CellRanger v3.1, Seurat v.3.1.4, R (v.3.6.2), VISION R package (v.2.1.0), and Monocle3 (v.0.2.3.0). Multiplex IHC was analysed using Phenochart (v.1.0.12), inFORM software (v2.4.8), phenoptr (v.0.2.5), and phenoptrReports (v.0.2.6).

For manuscripts utilizing custom algorithms or software that are central to the research but not yet described in published literature, software must be made available to editors/reviewers. We strongly encourage code deposition in a community repository (e.g. GitHub). See the Nature Research [guidelines for submitting code & software](#) for further information.

Data

Policy information about [availability of data](#)

All manuscripts must include a [data availability statement](#). This statement should provide the following information, where applicable:

- Accession codes, unique identifiers, or web links for publicly available datasets
- A list of figures that have associated raw data
- A description of any restrictions on data availability

The following protein sequences were employed for predicting and generating HPV peptides: E2 (Uniprot P03120), E5 (UniprotP06927), E6 (Uniprot03126), and E7 (Uniprot P03129). scRNA-seq data are available in the NCBI Gene Expression Omnibus (GEO) database under the accession number GSE180268. Other relevant data are available from the corresponding authors upon reasonable request.

Field-specific reporting

Please select the one below that is the best fit for your research. If you are not sure, read the appropriate sections before making your selection.

- Life sciences Behavioural & social sciences Ecological, evolutionary & environmental sciences

For a reference copy of the document with all sections, see [nature.com/documents/nr-reporting-summary-flat.pdf](https://www.nature.com/documents/nr-reporting-summary-flat.pdf)

Life sciences study design

All studies must disclose on these points even when the disclosure is negative.

Sample size	Sample size for each experiment is described in the manuscript and is based on the availability of adequate samples. No sample size calculations were performed prior to the study.
Data exclusions	No data were excluded.
Replication	No data or experiments are excluded. No replication was performed on individual patient specimens given limited sample availability. However, analyses were performed over several batches of patients with similar results.
Randomization	No randomization was used in this study as no experimental treatments/groups were involved.
Blinding	Not applicable as this is a descriptive study and no interventions were tested.

Reporting for specific materials, systems and methods

We require information from authors about some types of materials, experimental systems and methods used in many studies. Here, indicate whether each material, system or method listed is relevant to your study. If you are not sure if a list item applies to your research, read the appropriate section before selecting a response.

Materials & experimental systems

n/a	Involved in the study
<input type="checkbox"/>	<input checked="" type="checkbox"/> Antibodies
<input checked="" type="checkbox"/>	<input type="checkbox"/> Eukaryotic cell lines
<input checked="" type="checkbox"/>	<input type="checkbox"/> Palaeontology
<input checked="" type="checkbox"/>	<input type="checkbox"/> Animals and other organisms
<input type="checkbox"/>	<input checked="" type="checkbox"/> Human research participants
<input checked="" type="checkbox"/>	<input type="checkbox"/> Clinical data

Methods

n/a	Involved in the study
<input checked="" type="checkbox"/>	<input type="checkbox"/> ChIP-seq
<input type="checkbox"/>	<input checked="" type="checkbox"/> Flow cytometry
<input checked="" type="checkbox"/>	<input type="checkbox"/> MRI-based neuroimaging

Antibodies

Antibodies used

The antibodies used for flow cytometry are detailed in Ext. Data Table 1.
The following antibodies were used for multiplex IHC:
anti-CD3 (clone F7.2.38, Dako, #M7254), CD8 (clone C8/144B, eBiosciences, #14-0085-82), CD20 (clone L26, Invitrogen, #14-0202-82), TCF-1 (clone C63D9, Cell Signaling Technologies, #2203S), PD-1 (clone D4W2J, Cell Signaling Technologies, #86163S), and cytokeratin (clone AE1/3, Dako, #GA053)

Validation

The primary antibodies used in this study are widely used and well validated. The mentioned antibodies are tested by immunofluorescent staining with flow cytometric analysis by the manufacturer. The following information is available through the manufacturers' websites:

- anti-CCR7 staining of human peripheral blood lymphocytes by flow cytometry
- anti-CD3 staining of human peripheral blood lymphocytes by flow cytometry
- anti-CD4 staining of human peripheral blood lymphocytes cells by flow cytometry
- anti-CD8 staining of human peripheral blood lymphocytes by flow cytometry
- anti-CD14 staining of human peripheral blood mononuclear cells by flow cytometry
- anti-CD16 staining of human peripheral blood mononuclear cells by flow cytometry
- anti-CD25 staining of PHA-stimulated (day-3)-stimulated human peripheral blood lymphocytes by flow cytometry
- anti-CD28 staining of human peripheral blood lymphocytes by flow cytometry
- anti-CD39 staining of human peripheral blood lymphocytes by flow cytometry
- anti-CD45RA staining of human peripheral blood lymphocytes by flow cytometry
- anti-CD45RO staining of human peripheral blood lymphocytes by flow cytometry
- anti-CD127 staining of human peripheral blood lymphocytes by flow cytometry
- anti-GranzB staining of human peripheral blood mononuclear cells by flow cytometry
- anti-IFN- γ staining of PMA/ionomycin-stimulated human peripheral blood mononuclear cells by flow cytometry
- anti-Ki-67 staining of proliferating human MOLT-4 (T lymphoblastic leukemia, ATCC CRL-1582) cell line and non-cycling peripheral

blood mononuclear cells by flow cytometry
 anti-PD1 staining of PHA-stimulated (day-3)-stimulated human peripheral blood lymphocytes by flow cytometry
 anti-TCF-1 staining of Jurkat cells by flow cytometry
 anti-Tim-3 staining of Th1-polarized human peripheral blood lymphocytes by flow cytometry
 anti-TNF-alpha staining of PMA/ionomycin-stimulated human peripheral blood lymphocytes by flow cytometry
 anti-TOX staining of C57Bl/6 mice thymocytes by flow cytometry

The antibodies used for multiplex IHC analyses were validated by the manufacturers for immunohistochemistry.

Human research participants

Policy information about [studies involving human research participants](#)

Population characteristics	Male and female patients (age 44-75) diagnosed with HNSCC and undergoing surgery were recruited. All patients had previously untreated locally advanced disease at the time of surgery, presented with a locally metastatic lymph node and were classified as Stage I by the AJCC 8th edition staging guide.
Recruitment	Patients undergoing surgery in the Department of Otolaryngology at Emory University Hospital were consented to collect specimens. Recruitment was focused on patients presenting with detectable primary tumours and metastasis to lymphnodes.
Ethics oversight	HNSCC patients undergoing surgery were recruited in accordance with an approved Emory University Institutional Review Board protocol (WINSHIP4008-17), with all patients providing informed consent.

Note that full information on the approval of the study protocol must also be provided in the manuscript.

Flow Cytometry

Plots

Confirm that:

- The axis labels state the marker and fluorochrome used (e.g. CD4-FITC).
- The axis scales are clearly visible. Include numbers along axes only for bottom left plot of group (a 'group' is an analysis of identical markers).
- All plots are contour plots with outliers or pseudocolor plots.
- A numerical value for number of cells or percentage (with statistics) is provided.

Methodology

Sample preparation	Tumour samples (primary/metastatic) obtained from transoral robotic surgery and/or radical neck dissection were immediately collected and stored in Leibovitz's L-15 medium. Tissue samples were minced into small pieces and digested using an enzymatic cocktail of collagenase I, II, and IV, elastase and DNase (Worthington). Lymphocytes were isolated by using a 44%/67% Percoll gradient. Peripheral blood samples were collected in sodium citrate CPT cell preparation tubes (BD) at time of surgery and processed immediately to obtain peripheral blood mononuclear cells (PBMCs) and plasma. After lysis of red blood cells using ACK Lysing buffer, PBMCs were washed 4 times with Dulbecco's phosphate buffered saline without calcium and magnesium (DPBS) plus 2% fetal calf serum (FCS). Tissue lymphocytes and PBMCs were cryopreserved in 90% FCS with 10% DMSO, and eventually stored in liquid nitrogen.
Instrument	FACS data was collected on a BD LSR-II, FACS Canto-II, FACSymphony A5 or during cell sorting on a FACSaria II
Software	FACS data was collected using BD FACSDiva and analysed with FlowJo V10.6.1
Cell population abundance	Post-sort purity was analysed for samples with more than 5000 target cells collected. In all cases purity was greater than 98%.
Gating strategy	Gating strategy is shown in Extended Data section.

Tick this box to confirm that a figure exemplifying the gating strategy is provided in the Supplementary Information.